European Journal of Mechanics / A Solids 105 (2024) 105219

Contents lists available at ScienceDirect

European Journal of Mechanics / A Solids

journal homepage: www.elsevier.com/locate/ejmsol

Full length article

Effective double-poroelasticity derived via homogenization of two non-interacting solid phases percolated by a viscous fluid

Laura Miller, Raimondo Penta *

University of Glasgow, School of Mathematics and Statistics, Mathematics and Statistics Building, Glasgow, G12 8QQ, UK

ARTICLE INFO

Keywords:
Multiscale modelling
Poroelasticity
Homogenization
Fluid–structure interaction

ABSTRACT

This work carries out the derivation of the governing equations for a composite material that has the following microstructure. Our microstructure possesses an elastic matrix that has an incompressible Newtonian fluid flowing in the pores and then the latter is additionally reinforced by an elastic network that is fully surrounded by the fluid. We exploit the length scale separation that exists in the system between the microscale and the overall size of the material to apply the asymptotic homogenization technique. The resulting model comprises additional terms and equations to account for the discontinuity between the elastic phases, and reduces to more standard poroelastic formulations only when the two elastic phases are in contact. The coefficients of the novel model are to be computed by solving appropriate periodic cell differential problems. The coefficients encode the details of the geometry and stiffness of the microstructure. The model is applicable to a variety of scenarios, such as artificial constructs and biomaterials.

1. Introduction

Materials which possess a porous elastic matrix with a permeating fluid flow can be modelled using the Theory of Poroelasticity. This theory was developed by Biot (1955, 1956a,b, 1962) and is used to determine the effective behaviour of these types of materials. The theory can be applied if the interactions between the elastic matrix and the fluid take place at a scale where both of the phases are distinct. There are many real-world examples of where this modelling framework has been applied. The approach has been taken for hard hierarchical tissues, such as bones and tendons (Cowin, 1999; Weiner and Wagner, 1998). It can also be useful in soft tissues such as in the interstitial matrix in healthy and tumorous biological tissues (Bottaro and Ansaldi, 2012), the heart muscle (myocardium) (May-Newman and McCulloch, 1998; Cookson et al., 2012) and artery walls (see e.g Bukac et al., 2015; Jayaraman, 1983; Klanchar and Tarbell, 1987; Zakerzadeh and Zunino, 2014). There are also examples outwith human or animal biology and these include artificial constructs and biomaterials (Chalasani et al., 2007; Karageorgiou and Kaplan, 2005; Flessner, 2001) and in geomechanics and hydrology (Xu et al., 2022; Carrillo and Bourg, 2019). The original theory was considered for soil and rock mechanics (Kümpel, 1991; Wang, 2017).

Porous media are generally characterized by a variety of features found over multiple scales. The pores in the material are small and are visible on a fine scale which we can describe as the *porescale*. It is at this scale that the interactions between the various solid phases and the fluid take place. The porescale is much smaller than the scale at which we describe the whole material (which we will denote the *macroscale*). At the macroscale we no longer can see the pores or the interactions of the different phases taking place.

In order to fully understand the effective macroscale properties of the material we wish to relate them to the attributes and interactions taking place on the porescale, without creating a huge computational cost. To do this we can create a coupled fluid–structure interaction problem describing the material on the porescale and this can be used in an upscaling process which will lead to the macroscale governing equations. There exists a variety of approaches to the upscaling which are classified as *homogenization techniques*. These homogenization techniques include mixture theory, effective medium theory, volume averaging and asymptotic homogenization. For a complete review and discussion of these techniques see Hori and Nemat-Nasser (1999) and Davit et al. (2013). Each of these techniques has a variety of advantages and benefits depending on the features of the material that are to be modelled and the desired output from the final model.

The asymptotic homogenization technique, developed in Auriault et al. (2010), Holmes (2012), Mei and Vernescu (2010), Bakhvalov and Grigory (1989) and Bakhvalov and Panasenko (2012) has been applied to derive Biot's equations of poroelasticity in Burridge and Keller (1981), Lévy (1979), Wang (2017), Penta et al. (2020). The theory has been further developed in many ways, such as to include

* Corresponding author.
E-mail address: Raimondo.Penta@glasgow.ac.uk (R. Penta).

https://doi.org/10.1016/j.euromechsol.2023.105219
Received 9 March 2023; Received in revised form 28 November 2023; Accepted 28 December 2023
Available online 3 January 2024
0997-7538/© 2024 The Authors. Published by Elsevier Masson SAS. This is an open access article under the CC BY license (http://creativecommons.org/licenses/by/4.0/).

growth of poroelastic materials (Penta et al., 2014), the addition of vascularized poroelastic materials (Penta and Merodio, 2017), poroelastic composites (Miller and Penta, 2020) and double poroelastic materials (Miller and Penta, 2021a). Another development has been in considering poroelastic materials undergoing large deformations such as active poroelastic materials (Collis et al., 2017) and nonlinear poroelastic composites (Miller and Penta, 2021b). The poroelastic models derived via asymptotic homogenization have been numerically investigated such as in Dehghani et al. (2018) where the role of porosity and microscale solid matrix compressibility on the mechanical behaviour of poroelastic materials is considered. The macroscale behaviour was also investigated in Dehghani et al. (2020). More recently the role of the microstructure of a poroelastic material on the resulting elastic parameters has been investigated in Miller and Penta (2023b) and then further specialized to investigate the structural changes involved in myocardial infarction (Miller and Penta, 2023a). The technique has been used to address double porosity in fluid-saturated elastic media in Rohan et al. (2015). This model considers the interactions occurring between a poroelastic phase and an interconnected fluid phase and provides an application of the framework to compact bone in Rohan et al. (2012). This model is also applicable to tissue perfusion and has been used to carry out investigations in Rohan and Cimrman (2010) and Rohan et al. (2021).

In this work, we will apply the asymptotic homogenization technique to the fluid-structure interaction (FSI) problem that describes the interplay between a porous elastic matrix that has an incompressible Newtonian fluid flowing in the pores with elastic network reinforcing the material that is also fully surrounded by the fluid. This means that the elastic matrix and the fibre network are both interacting with the fluid flow. For example, this type of structure can be found in the myocardium or brain. When the vasculature supplying the heart or brain becomes diseased via, for example, a build up of atherosclerosis, blood clot or aneurysm, this geometry can be used. The blood vessels embedded within the myocardium are represented as the interconnected fluid-filled pore phase. The additional elastic phase can be a medical device, such as a stent or device to remove clots (Tsivgoulis et al., 2016), that treats disease or damage in the vessel (Kolodgie et al., 2007). It is also applicable in the context of bone remodelling where the process is regulated by mechanosensitive bone cells called osteocytes. These osteocytes are immersed in the interstitial fluid and can be found in the microscale pores (Perrin et al., 2019; Sánchez et al., 2021).

We consider the material at the scale where the various solid phases and the pores are clearly visible and denote this scale as the microscale. This scale is much smaller than the entire material which we denote as the macroscale. By using the asymptotic homogenization technique to upscale we account for the continuity of stresses and velocities across the fluid–solid interfaces. That is, between the matrix and the fluid, and the fibres and the fluid. We note that there is no continuity of the stresses or displacements between the matrix and the fibres since there is no contact points between them. It is important to note that the two solid phases are fully decoupled from each other, and therefore we are considering two elastic materials separated by a fluid. We can consider this a poroelastic problem for each solid and fluid when ignoring the other solid constituent. We note that this is not the coupling of two poroelastic materials but of three distinct phases: matrix, fluid, fibres. The derived novel, quasi-static macroscale model cannot be deduced as a special case of Miller and Penta (2020) for poroelastic composites as it is no longer a Biot-type model due to the additional equation required to close the system. The novel model contains additional terms to account for the discontinuity between the different elastic phases and the influence on the fluid that is constrained between them. We are able to recover (Miller and Penta, 2020) by assuming that in fact the matrix and the fibres are in contact and that we have the continuity of the elastic displacements. The coefficients of the model encode the properties of the microstructure and are to be computed by solving the microscale differential problems that arise as a result of applying the asymptotic homogenization technique.

A similar approach has been taken in Santos et al. (2006) where fractures of porous media are investigated using the asymptotic homogenization technique. The structure in their work involves two different elastic phases and a fluid phase but is restricted to a simplified geometry where one of the solid phases envelops the other. This means that there is only one solid phase (the internal one) in contact with the fluid. The upscaling is carried out assuming a non-wielded interface between the two solid phases. This differs dramatically from our geometry as we have a complete discontinuity between the elastic phases which leads to both elastic phases having contact with the fluid.

The paper is organized as follows. We begin by introducing the FSI problem in Section 2. This problem describes the interactions between the elastic matrix, the elastic fibre network, and the fluid that is flowing in the space between the matrix and the network. In Section 3, we perform a multiscale analysis of the FSI problem detailed in Section 2. The given problem is a system partial differential equations (PDEs). In Section 3, we derive the new macroscale model which governs the homogenized mechanical behaviour of poroelastic composites. In Section 4, we discuss the macroscale results and recover previously known works as limit cases. We also provide some potential applications for the model in Section 5. In Section 6, we provide the conclusions to our work and provide further perspectives.

2. The fluid–structure interaction problem (FSI)

In order to write our fluid–structure interaction problem we first define some sets. We define a set $\Omega \in \mathbb{R}^3$, and we let Ω be the union of a solid porous matrix Ω_{II}, an interconnected fluid flow Ω_{f}, and Ω_{I} which is a connected fibre network. We can write that $\bar{\Omega} = \bar{\Omega}_{\text{I}} \cup \bar{\Omega}_{\text{II}} \cup \bar{\Omega}_{\text{f}}$. For a 2D schematic diagram of the structure we are considering here see Fig. 1.

We begin our FSI problem with the balance equations for each of the solid domains Ω_{I} and Ω_{II}. We do not consider volume forces or inertia so the balance equations are,

$$\nabla \cdot \boldsymbol{\sigma}_{\text{I}} = 0 \quad \text{in} \quad \Omega_{\text{I}}, \tag{1}$$

and

$$\nabla \cdot \boldsymbol{\sigma}_{\text{II}} = 0 \quad \text{in} \quad \Omega_{\text{II}}. \tag{2}$$

In Eqs. (1)–(2) we have $\boldsymbol{\sigma}_{\text{I}}$ and $\boldsymbol{\sigma}_{\text{II}}$ and these denote the solid stress tensors for the fibre network Ω_{I} and the matrix Ω_{II}, respectively. We make the assumption that the matrix and fibre network are anisotropic, linear elastic solids. This means that they have the constitutive laws

$$\boldsymbol{\sigma}_{\text{I}} = \mathbb{C}_{\text{I}} \nabla \mathbf{u}_{\text{I}}, \tag{3}$$

$$\boldsymbol{\sigma}_{\text{II}} = \mathbb{C}_{\text{II}} \nabla \mathbf{u}_{\text{II}}, \tag{4}$$

where we have that $\mathbf{u}_{\text{I}}$ and $\mathbf{u}_{\text{II}}$ are the elastic displacement in the fibre and the matrix, respectively.

Within the constitutive laws (3)–(4) the fourth rank tensors $\mathbb{C}_{\text{I}}$ and $\mathbb{C}_{\text{II}}$ appear. These are the elasticity tensors for the elastic fibre and the matrix. These tensors have the corresponding components C^{I}_{ijkl} and C^{II}_{ijkl}, for $i, j, k, l = 1, 2, 3$. Each of the elasticity tensors $\mathbb{C}_{\text{I}}$ and $\mathbb{C}_{\text{II}}$ possess right minor and major symmetries, these are

$$C^{\text{I}}_{ijkl} = C^{\text{I}}_{ijlk}; \quad C^{\text{II}}_{ijkl} = C^{\text{II}}_{ijlk}, \tag{5}$$

$$C^{\text{I}}_{ijkl} = C^{\text{I}}_{klij}; \quad C^{\text{II}}_{ijkl} = C^{\text{II}}_{klij}, \tag{6}$$

We have that the left minor symmetries also exist, we see this by combining (5)–(6). By using the left minor symmetries in the constitutive Eqs. (3)–(4) we car rewrite them as follows

$$\boldsymbol{\sigma}_{\text{I}} = \mathbb{C}_{\text{I}} \xi(\mathbf{u}_{\text{I}}), \tag{7}$$

$$\boldsymbol{\sigma}_{\text{II}} = \mathbb{C}_{\text{II}} \xi(\mathbf{u}_{\text{II}}), \tag{8}$$

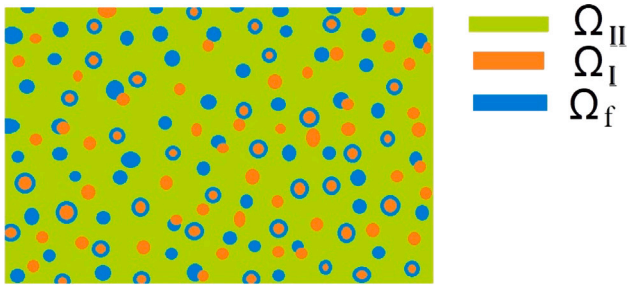

Fig. 1. A 2D sketch representing a cross-section of the three-dimensional domain Ω. The fluid phase is represented in blue, the porous matrix in green, and the fibres in orange. In this diagram the inclusions have three different placements, that is embedded in the matrix, embedded in the fluid or in contact with both. In this work we consider that the fibres that are fully surrounded by the fluid. (For interpretation of the references to colour in this figure legend, the reader is referred to the web version of this article.)

where we define

$$\xi(\bullet) = \frac{\nabla(\bullet) + (\nabla(\bullet))^T}{2} \tag{9}$$

which is the symmetric part of the gradient operator.

We also require a balance equation for the fluid domain. This is given as

$$\nabla \cdot \boldsymbol{\sigma}_{\mathrm{f}} = 0 \quad \text{in} \quad \Omega_{\mathrm{f}}, \tag{10}$$

and we have that $\boldsymbol{\sigma}_{\mathrm{f}}$ is the fluid stress tensor. We are making the assumption that our fluid is incompressible and Newtonian, and so therefore has the constitutive equation

$$\boldsymbol{\sigma}_{\mathrm{f}} = -p\mathbf{I} + \mu\xi(\mathbf{v}) \tag{11}$$

where we have $\mathbf{v}$ as the fluid velocity, p is the pressure and μ the viscosity of the fluid. Since the fluid is incompressible we require the incompressibility constraint

$$\nabla \cdot \mathbf{v} = 0 \quad \text{in} \quad \Omega_{\mathrm{f}}. \tag{12}$$

By using the constitutive law (11) in the balance Eq. (10) with the incompressibility constraint (12) we obtain the Stokes' problem

$$\mu\nabla^2\mathbf{v} = \nabla p \quad \text{in} \quad \Omega_{\mathrm{f}}. \tag{13}$$

To close the FSI problem we require some interface conditions between the fluid and solid phases. The interface between the fluid phase and the fibre is defined as $\Gamma_{\mathrm{I}} := \partial\Omega_{\mathrm{I}} \cap \partial\Omega_{\mathrm{f}}$ and the interface between the matrix and the fluid is defined as $\Gamma_{\mathrm{II}} := \partial\Omega_{\mathrm{II}} \cap \partial\Omega_{\mathrm{f}}$. Across each of these interfaces we impose the continuity of velocities and stresses, that is

$$\dot{\mathbf{u}}_{\mathrm{I}} = \mathbf{v} \quad \text{on} \quad \Gamma_{\mathrm{I}}, \tag{14}$$

$$\boldsymbol{\sigma}_{\mathrm{f}}\mathbf{n}_{\mathrm{I}} = \boldsymbol{\sigma}_{\mathrm{I}}\mathbf{n}_{\mathrm{I}} \quad \text{on} \quad \Gamma_{\mathrm{I}}, \tag{15}$$

$$\dot{\mathbf{u}}_{\mathrm{II}} = \mathbf{v} \quad \text{on} \quad \Gamma_{\mathrm{II}}, \tag{16}$$

$$\boldsymbol{\sigma}_{\mathrm{f}}\mathbf{n}_{\mathrm{II}} = \boldsymbol{\sigma}_{\mathrm{II}}\mathbf{n}_{\mathrm{II}} \quad \text{on} \quad \Gamma_{\mathrm{II}}. \tag{17}$$

We have that $\dot{\mathbf{u}}_{\mathrm{I}}$ and $\dot{\mathbf{u}}_{\mathrm{II}}$ are the solid velocities for each fibre Ω_{I} and the matrix Ω_{II}, respectively. The unit normal vectors to each of the interfaces Γ_{I} and Γ_{II} are given as $\mathbf{n}_{\mathrm{I}}$ and $\mathbf{n}_{\mathrm{II}}$, respectively.

In the next section we perform a multiscale analysis of the FSI problem we have introduced. We begin by non-dimensionalizing the partial differential equations (PDEs) described in this section. We will then explain the two well-separated length scales that exist in our system which allows us to apply the asymptotic homogenization technique to the non-dimensional FSI problem. Then we will derive effective balance equations that describe the material.

3. Multiple scales analysis of the FSI problem

We begin by summarizing the fluid–structure interaction problem that we introduced in the previous section and then we will perform a multiple scales analysis. The problem is given by

$$\nabla \cdot \boldsymbol{\sigma}_{\mathrm{I}} = 0 \quad \text{in} \quad \Omega_{\mathrm{I}}, \tag{18}$$

$$\nabla \cdot \boldsymbol{\sigma}_{\mathrm{II}} = 0 \quad \text{in} \quad \Omega_{\mathrm{II}}, \tag{19}$$

$$\nabla \cdot \boldsymbol{\sigma}_{\mathrm{f}} = 0 \quad \text{in} \quad \Omega_{\mathrm{f}}, \tag{20}$$

$$\nabla \cdot \mathbf{v} = 0 \quad \text{in} \quad \Omega_{\mathrm{f}}, \tag{21}$$

$$\dot{\mathbf{u}}_{\mathrm{I}} = \mathbf{v} \quad \text{on} \quad \Gamma_{\mathrm{I}}, \tag{22}$$

$$\dot{\mathbf{u}}_{\mathrm{II}} = \mathbf{v} \quad \text{on} \quad \Gamma_{\mathrm{II}}, \tag{23}$$

$$\boldsymbol{\sigma}_{\mathrm{f}}\mathbf{n}_{\mathrm{I}} = \boldsymbol{\sigma}_{\mathrm{I}}\mathbf{n}_{\mathrm{I}} \quad \text{on} \quad \Gamma_{\mathrm{I}}, \tag{24}$$

$$\boldsymbol{\sigma}_{\mathrm{f}}\mathbf{n}_{\mathrm{II}} = \boldsymbol{\sigma}_{\mathrm{II}}\mathbf{n}_{\mathrm{II}} \quad \text{on} \quad \Gamma_{\mathrm{II}}. \tag{25}$$

Using the constitutive laws for the fibre network, matrix and the fluid (7), (8), and (11), and applying the incompressibility constraint (21), allows the balance Eqs. (18), (19), and (20) to be rewritten as

$$\nabla \cdot (\mathbb{C}_{\mathrm{I}}\xi(\mathbf{u}_{\mathrm{I}})) = 0 \quad \text{in} \quad \Omega_{\mathrm{I}} \tag{26}$$

$$\nabla \cdot (\mathbb{C}_{\mathrm{II}}\xi(\mathbf{u}_{\mathrm{II}})) = 0 \quad \text{in} \quad \Omega_{\mathrm{II}} \tag{27}$$

$$\mu\nabla^2\mathbf{v} = \nabla p \quad \text{in} \quad \Omega_{\mathrm{f}}. \tag{28}$$

In order to close the problem (18)–(28) we must prescribe external boundary conditions on the boundary $\partial\Omega$. These conditions could be, for example, of Dirichlet–Neumann type, as noted in Ramírez-Torres et al. (2018). The conditions on the external boundary typically do not play a role in the derivation of results carried out by formal asymptotic homogenization, although they are important in the context of rigorous two-scale convergence, see, e.g., Cioranescu and Donato (1999).

Our material can be characterized by two different length scales. We describe the average size of the whole material/domain Ω by length L and call this the *the macroscale*. We then have a second length scale where the matrix, fluid and fibres are clearly visible. We denote our second length by d and call this scale the *the microscale*. In order to emphasize the difference between the two scales, we will carry out a non-dimensional analysis of the FSI problem (18)–(28).

3.1. Non-dimensionalization of the FSI problem

We carry out the non-dimensionalization by assuming that our system has a reference pressure gradient C. We also use the standard parabolic profile for the fluid flowing in the pores. This choice is the classic one that ensures that a Newtonian fluid flowing in cylindrical pores is governed by the porous media flow equations. If we make a different choice for the velocity scaling then we would not obtain the correct effective behaviour of a fluid flowing through a porous matrix.

We therefore have the following

$$\begin{gathered} \mathbf{x} = L\mathbf{x}', \quad \mathbb{C}_{\mathrm{I}} = CL\mathbb{C}'_{\mathrm{I}}, \quad \mathbb{C}_{\mathrm{II}} = CL\mathbb{C}'_{\mathrm{II}}, \\ \mathbf{u}_{\mathrm{I}} = L\mathbf{u}'_{\mathrm{I}}, \quad \mathbf{u}_{\mathrm{II}} = L\mathbf{u}'_{\mathrm{II}}, \quad \mathbf{v} = \frac{Cd^2}{\mu}\mathbf{v}', \quad p = CLp'. \end{gathered} \tag{29}$$

The gradient operator is also scaled as

$$\nabla = \frac{1}{L}\nabla' \tag{30}$$

We can use (29) and (30) in (18)–(25), and we obtain the non-dimensional system

$$\nabla \cdot \boldsymbol{\sigma}_{\mathrm{I}} = 0 \quad \text{in} \quad \Omega_{\mathrm{I}} \tag{31}$$

$$\nabla \cdot \boldsymbol{\sigma}_{\mathrm{II}} = 0 \quad \text{in} \quad \Omega_{\mathrm{II}} \tag{32}$$

$$\nabla \cdot \boldsymbol{\sigma}_{\mathrm{f}} = 0 \quad \text{in} \quad \Omega_{\mathrm{f}} \tag{33}$$

$$\nabla \cdot \mathbf{v} = 0 \quad \text{in} \quad \Omega_{\mathrm{f}} \tag{34}$$

$$\dot{\mathbf{u}}_{\mathrm{I}} = \mathbf{v} \quad \text{on} \quad \Gamma_{\mathrm{I}} \tag{35}$$

$$\dot{\mathbf{u}}_{\mathrm{II}} = \mathbf{v} \quad \text{on} \quad \Gamma_{\mathrm{II}} \tag{36}$$

$$\boldsymbol{\sigma}_{\mathrm{f}}\mathbf{n}_{\mathrm{I}} = \boldsymbol{\sigma}_{\mathrm{I}}\mathbf{n}_{\mathrm{I}} \quad \text{on} \quad \Gamma_{\mathrm{I}} \tag{37}$$

$$\boldsymbol{\sigma}_{\mathrm{f}}\mathbf{n}_{\mathrm{II}} = \boldsymbol{\sigma}_{\mathrm{II}}\mathbf{n}_{\mathrm{II}} \quad \text{on} \quad \Gamma_{\mathrm{II}}. \tag{38}$$

Note that we drop the primes to simplify the notation. We must also non-dimensionalize the constitutive laws (7), (8), and (11), which become

$$\boldsymbol{\sigma}_{\mathrm{f}} = -p\mathrm{I} + \epsilon^2\xi(\mathbf{v}) \tag{39}$$

$$\boldsymbol{\sigma}_{\mathrm{I}} = \mathbb{C}_{\mathrm{I}}\xi(\mathbf{u}_{\mathrm{I}}) \tag{40}$$

$$\boldsymbol{\sigma}_{\mathrm{II}} = \mathbb{C}_{\mathrm{II}}\xi(\mathbf{u}_{\mathrm{II}}). \tag{41}$$

Using the non-dimensionalized constitutive laws we can rewrite the balance Eqs. (31)–(33) as

$$\epsilon^2\nabla^2\mathbf{v} = \nabla p \quad \text{in} \quad \Omega_{\mathrm{f}} \tag{42}$$

$$\nabla\cdot(\mathbb{C}_{\mathrm{I}}\xi(\mathbf{u}_{\mathrm{I}})) = 0 \quad \text{in} \quad \Omega_{\mathrm{I}} \tag{43}$$

$$\nabla\cdot(\mathbb{C}_{\mathrm{II}}\xi(\mathbf{u}_{\mathrm{II}})) = 0 \quad \text{in} \quad \Omega_{\mathrm{II}}, \tag{44}$$

where we can define

$$\epsilon = \frac{d}{L}. \tag{45}$$

Now that we have the non-dimensional system of PDEs (31)–(44) we are ready to introduce the asymptotic homogenization technique which we use to upscale the system by assuming that the microscale and the macroscale are both well separated.

3.2. The two-scale asymptotic homogenization technique

Here we will introduce the asymptotic homogenization technique and apply it to (31)–(44) to derive the macroscale model. We must make the assumption that the microscale (the length associated with where we can clearly identify the fluid, inclusions/fibres and matrix), denoted by d, is much smaller that the average size of the material, denoted L. That is,

$$\epsilon = \frac{d}{L} \ll 1. \tag{46}$$

We want to capture the microscale variations of each of the fields so we introduce the spatial variable

$$\mathbf{y} = \frac{\mathbf{x}}{\epsilon}. \tag{47}$$

We consider the spatial variables $\mathbf{x}$ and $\mathbf{y}$ formally independent where $\mathbf{x}$ represents the macroscale and $\mathbf{y}$ the microscale. We also transform the gradient operator, by means of the chain rule, as

$$\nabla \to \nabla_{\mathbf{x}} + \frac{1}{\epsilon}\nabla_{\mathbf{y}}. \tag{48}$$

We make the assumption that all fields in (31)–(44) are functions of both $\mathbf{x}$ and $\mathbf{y}$ and that they can all be written as a power series in ϵ, i.e.

$$\varphi^{\epsilon}(\mathbf{x},\mathbf{y},t) = \sum_{l=0}^{\infty}\varphi^{(l)}(\mathbf{x},\mathbf{y},t)\epsilon^l, \tag{49}$$

where φ is an individual field appearing in (31)–(44).

Remark 1 (*Porescale Periodicity*)**.** We make the assumption that every field $\varphi^{(l)}$ in our present analysis is $\mathbf{y}$-periodic. By assuming this the analysis of the microstructure can take place on a single periodic cell. It allows the microscale differential problems arising from the asymptotic homogenization technique to be solved on a finite subset of the domain. This assumption need not be made as it is possible to proceed by assuming local boundedness of fields only. Some examples of this are found in Burridge and Keller (1981) and Penta and Gerisch (2017).

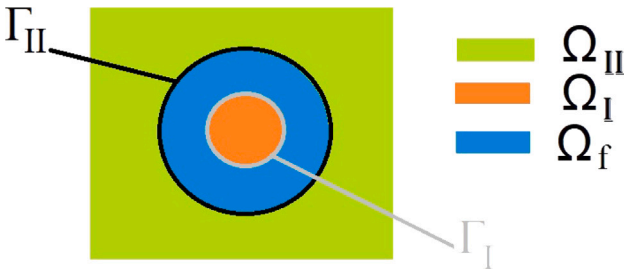

Fig. 2. This is a sketch of a 2D cross-section of the periodic cell that we focus on. We have the fibre network shown in orange that is fully embedded in the fluid shown in blue, and the matrix is shown in green. We highlight the interfaces Γ_{I} and Γ_{II} between the phases. (For interpretation of the references to colour in this figure legend, the reader is referred to the web version of this article.)

Remark 2 (*Macroscopic Uniformity*)**.** We know that the microscale geometry can change with respect to individual points on the macroscale. This has been considered in Penta et al. (2014), Burridge and Keller (1981), Holmes (2012), Penta and Gerisch (2015) and Dalwadi et al. (2015). To make the derivation of the model simpler this dependence on the macroscale is generally neglected. That is we assume that at every macroscale point the microscale will be the same, or equivalently the microscale geometry does not depend on $\mathbf{x}$. This property is called macroscopic uniformity. We use this property in this work. This means that we have the following result for differentiation under the integral sign

$$\int_{\Omega}\nabla_{\mathbf{x}}\cdot(\bullet)\mathrm{d}\mathbf{y} = \nabla_{\mathbf{x}}\cdot\int_{\Omega}(\bullet)\mathrm{d}\mathbf{y}, \tag{50}$$

where $(\bullet)$ is a tensor or a vector quantity.

Remark 3 (*Periodic Cell*)**.** We make the identification between the domain Ω and the corresponding periodic cell, where the subphase, matrix, and fluid cell portions are denoted by Ω_{I}, Ω_{II}, and Ω_{f}, respectively. We also have the interfaces between the different phases are then denoted by $\Gamma_{\mathrm{I}} := \partial\Omega_{\mathrm{I}}\cap\partial\Omega_{\mathrm{f}}$, $\Gamma_{\mathrm{II}} := \partial\Omega_{\mathrm{II}}\cap\partial\Omega_{\mathrm{f}}$ with corresponding unit normal vectors $\mathbf{n}_{\mathrm{I}}$ and $\mathbf{n}_{\mathrm{II}}$. This cell is shown in Fig. 3. We note that $|\Omega| = |\Omega_{\mathrm{f}}| + |\Omega_{\mathrm{I}}| + |\Omega_{\mathrm{II}}|$ is the domain volume which since we are assuming a unit cell is equal to 1. Now that we have this periodic cell (cube) Fig. 3, we have periodic boundary conditions applied on all the faces, where each face contains a portion of all the phases as shown in Fig. 2.

3.3. Application of the asymptotic homogenization technique

We now apply the assumptions (48) and (49) of the asymptotic homogenization technique to Eqs. (31)–(44). By also accounting for periodicity we obtain the following multiscale system of PDEs

$$\nabla_{\mathbf{y}}\cdot\boldsymbol{\sigma}^{\epsilon}_{\mathrm{I}} + \epsilon\nabla_{\mathbf{x}}\cdot\boldsymbol{\sigma}^{\epsilon}_{\mathrm{I}} = 0 \quad \text{in} \quad \Omega_{\mathrm{I}} \tag{51}$$

$$\nabla_{\mathbf{y}}\cdot\boldsymbol{\sigma}^{\epsilon}_{\mathrm{II}} + \epsilon\nabla_{\mathbf{x}}\cdot\boldsymbol{\sigma}^{\epsilon}_{\mathrm{II}} = 0 \quad \text{in} \quad \Omega_{\mathrm{II}} \tag{52}$$

$$\nabla_{\mathbf{y}}\cdot\boldsymbol{\sigma}^{\epsilon}_{\mathrm{f}} + \epsilon\nabla_{\mathbf{x}}\cdot\boldsymbol{\sigma}^{\epsilon}_{\mathrm{f}} = 0 \quad \text{in} \quad \Omega_{f} \tag{53}$$

$$\nabla_{\mathbf{y}}\cdot\mathbf{v}^{\epsilon} + \epsilon\nabla_{\mathbf{x}}\cdot\mathbf{v}^{\epsilon} = 0 \quad \text{in} \quad \Omega_{f} \tag{54}$$

$$\dot{\mathbf{u}}^{\epsilon}_{\mathrm{I}} = \mathbf{v}^{\epsilon} \quad \text{on} \quad \Gamma_{\mathrm{I}} \tag{55}$$

$$\dot{\mathbf{u}}^{\epsilon}_{\mathrm{II}} = \mathbf{v}^{\epsilon} \quad \text{on} \quad \Gamma_{\mathrm{II}} \tag{56}$$

$$\boldsymbol{\sigma}^{\epsilon}_{\mathrm{f}}\mathbf{n}_{\mathrm{I}} = \boldsymbol{\sigma}^{\epsilon}_{\mathrm{I}}\mathbf{n}_{\mathrm{I}} \quad \text{on} \quad \Gamma_{\mathrm{I}} \tag{57}$$

$$\boldsymbol{\sigma}^{\epsilon}_{\mathrm{f}}\mathbf{n}_{\mathrm{II}} = \boldsymbol{\sigma}^{\epsilon}_{\mathrm{II}}\mathbf{n}_{\mathrm{II}} \quad \text{on} \quad \Gamma_{\mathrm{II}} \tag{58}$$

The multiscale expansion of the constitutive equations for $\boldsymbol{\sigma}^{\epsilon}_{\mathrm{f}}$, $\boldsymbol{\sigma}^{\epsilon}_{\mathrm{I}}$, $\boldsymbol{\sigma}^{\epsilon}_{\mathrm{II}}$, are

$$\boldsymbol{\sigma}^{\epsilon}_{\mathrm{f}} = -p^{\epsilon}\mathrm{I} + \epsilon\xi_{\mathbf{y}}(\mathbf{v}^{\epsilon}) + \epsilon^2\xi_{\mathbf{x}}(\mathbf{v}^{\epsilon}) \tag{59}$$

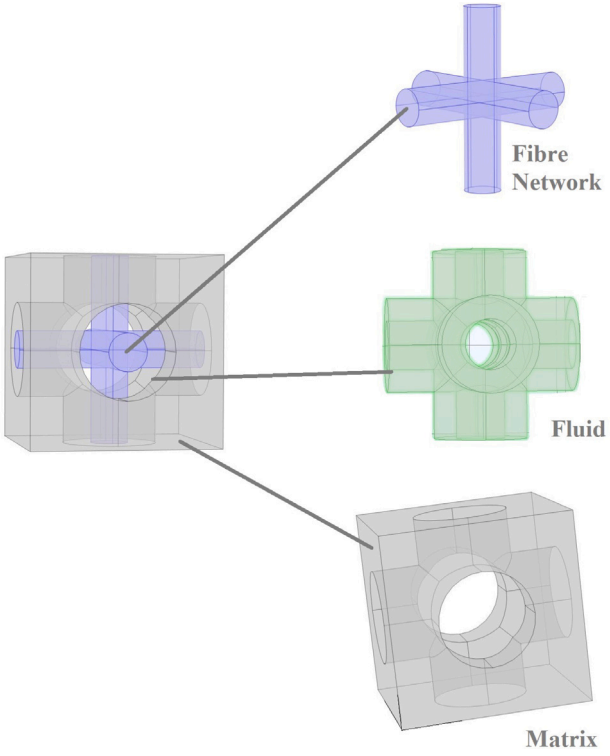

Fig. 3. This is a sketch of the 3D periodic cell that we focus on. We have the interconnected 3 cylinders creating the fibre network that is fully embedded in the fluid as shown by the holes in the fluid section and then we have the matrix.

$$\epsilon\boldsymbol{\sigma}_{\mathrm{I}}^{\epsilon} = \mathbb{C}_{\mathrm{I}}\xi_{\mathbf{y}}(\mathbf{u}_{\mathrm{I}}^{\epsilon}) + \epsilon\mathbb{C}_{\mathrm{I}}\xi_{\mathbf{x}}(\mathbf{u}_{\mathrm{I}}^{\epsilon}) \tag{60}$$

$$\epsilon\boldsymbol{\sigma}_{\mathrm{II}}^{\epsilon} = \mathbb{C}_{\mathrm{II}}\xi_{\mathbf{y}}(\mathbf{u}_{\mathrm{II}}^{\epsilon}) + \epsilon\mathbb{C}_{\mathrm{II}}\xi_{\mathbf{x}}(\mathbf{u}_{\mathrm{II}}^{\epsilon}), \tag{61}$$

and the balance equations become

$$\begin{aligned}&\nabla_{\mathbf{y}}\cdot(\mathbb{C}_{\mathrm{I}}\xi_{\mathbf{y}}(\mathbf{u}_{\mathrm{I}}^{\epsilon})) + \epsilon\nabla_{\mathbf{y}}\cdot(\mathbb{C}_{\mathrm{I}}\xi_{\mathbf{x}}(\mathbf{u}_{\mathrm{I}}^{\epsilon})) + \\ &\epsilon\nabla_{\mathbf{x}}\cdot(\mathbb{C}_{\mathrm{I}}\xi_{\mathbf{y}}(\mathbf{u}_{\mathrm{I}}^{\epsilon})) + \epsilon^2\nabla_{\mathbf{x}}\cdot(\mathbb{C}_{\mathrm{I}}\xi_{\mathbf{x}}(\mathbf{u}_{\mathrm{I}}^{\epsilon})) = 0 \quad \text{in} \quad \Omega_{\mathrm{I}}\end{aligned} \tag{62}$$

$$\begin{aligned}&\nabla_{\mathbf{y}}\cdot(\mathbb{C}_{\mathrm{II}}\xi_{\mathbf{y}}(\mathbf{u}_{\mathrm{II}}^{\epsilon})) + \epsilon\nabla_{\mathbf{y}}\cdot(\mathbb{C}_{\mathrm{II}}\xi_{\mathbf{x}}(\mathbf{u}_{\mathrm{II}}^{\epsilon})) + \\ &\epsilon\nabla_{\mathbf{x}}\cdot(\mathbb{C}_{\mathrm{II}}\xi_{\mathbf{y}}(\mathbf{u}_{\mathrm{II}}^{\epsilon})) + \epsilon^2\nabla_{\mathbf{x}}\cdot(\mathbb{C}_{\mathrm{II}}\xi_{\mathbf{x}}(\mathbf{u}_{\mathrm{II}}^{\epsilon})) = 0 \quad \text{in} \quad \Omega_{\mathrm{II}}\end{aligned} \tag{63}$$

$$\begin{aligned}&\epsilon^3\nabla_{\mathbf{x}}^2\mathbf{v}^{\epsilon} + \epsilon^2\nabla_{\mathbf{x}}\cdot(\nabla_{\mathbf{y}}\mathbf{v}^{\epsilon}) + \epsilon^2\nabla_{\mathbf{y}}\cdot(\nabla_{\mathbf{x}}\mathbf{v}^{\epsilon}) + \epsilon\nabla_{\mathbf{y}}^2\mathbf{v}^{\epsilon} \\ &= \nabla_{\mathbf{y}}p^{\epsilon} + \epsilon\nabla_{\mathbf{x}}p^{\epsilon} \quad \text{in} \quad \Omega_f\end{aligned} \tag{64}$$

We use the assumption that all fields can be written as power series of the type (49) in (51)–(64). We will equate the coefficients of ϵ^l for $l = 0, 1, \ldots$ to derive the macroscale model, which will therefore be in terms of the relevant leading (zero-th) order fields. If a component in the asymptotic expansion retains dependence on the microscale, we can apply the integral average, given by

$$\langle\varphi\rangle_i = \frac{1}{|\Omega|}\int_{\Omega_i}\varphi(\mathbf{x},\mathbf{y},t)d\mathbf{y} \quad i = f, \mathrm{I}, \mathrm{II} \tag{65}$$

We note that $|\Omega| = |\Omega_{\mathrm{f}}| + |\Omega_{\mathrm{I}}| + |\Omega_{\mathrm{II}}|$ is the domain volume. Since we have $\mathbf{y}$-periodicity, the integral average can be performed over one representative cell and so (65) is a cell average.

Equating coefficients of ϵ^0 in (51)–(58) we obtain

$$\nabla_{\mathbf{y}}\cdot\boldsymbol{\sigma}_{\mathrm{I}}^{(0)} = 0 \qquad \text{in} \quad \Omega_{\mathrm{I}} \tag{66}$$

$$\nabla_{\mathbf{y}}\cdot\boldsymbol{\sigma}_{\mathrm{II}}^{(0)} = 0 \qquad \text{in} \quad \Omega_{\mathrm{II}} \tag{67}$$

$$\nabla_{\mathbf{y}}\cdot\boldsymbol{\sigma}_{\mathrm{f}}^{(0)} = 0 \qquad \text{in} \quad \Omega_{\mathrm{f}} \tag{68}$$

$$\nabla_{\mathbf{y}}\cdot\mathbf{v}^{(0)} = 0 \qquad \text{in} \quad \Omega_{\mathrm{f}} \tag{69}$$

$$\dot{\mathbf{u}}_{\mathrm{I}}^{(0)} = \mathbf{v}^{(0)} \qquad \text{on} \quad \Gamma_{\mathrm{I}} \tag{70}$$

$$\dot{\mathbf{u}}_{\mathrm{II}}^{(0)} = \mathbf{v}^{(0)} \qquad \text{on} \quad \Gamma_{\mathrm{II}} \tag{71}$$

$$\boldsymbol{\sigma}_{\mathrm{f}}^{(0)}\mathbf{n}_{\mathrm{I}} = \boldsymbol{\sigma}_{\mathrm{I}}^{(0)}\mathbf{n}_{\mathrm{I}} \qquad \text{on} \quad \Gamma_{\mathrm{I}} \tag{72}$$

$$\boldsymbol{\sigma}_{\mathrm{f}}^{(0)}\mathbf{n}_{\mathrm{II}} = \boldsymbol{\sigma}_{\mathrm{II}}^{(0)}\mathbf{n}_{\mathrm{II}} \qquad \text{on} \quad \Gamma_{\mathrm{II}} \tag{73}$$

The coefficient of ϵ^0 in the constitutive Eqs. (59)–(61) for $\boldsymbol{\sigma}_{\mathrm{f}}^{\epsilon}$, $\boldsymbol{\sigma}_{\mathrm{I}}^{\epsilon}$, $\boldsymbol{\sigma}_{\mathrm{II}}^{\epsilon}$ are

$$\boldsymbol{\sigma}_{\mathrm{f}}^{(0)} = -p^{(0)}\mathrm{I} \qquad \text{in} \quad \Omega_{\mathrm{f}} \tag{74}$$

$$\mathbb{C}_{\mathrm{I}}\xi_{\mathbf{y}}(\mathbf{u}_{\mathrm{I}}^{(0)}) = 0 \qquad \text{in} \quad \Omega_{\mathrm{I}} \tag{75}$$

$$\mathbb{C}_{\mathrm{II}}\xi_{\mathbf{y}}(\mathbf{u}_{\mathrm{II}}^{(0)}) = 0 \qquad \text{in} \quad \Omega_{\mathrm{II}} \tag{76}$$

while the balance Eqs. (62)–(64) have coefficients of ϵ^0 given by

$$\nabla_{\mathbf{y}}\cdot(\mathbb{C}_{\mathrm{I}}\xi_{\mathbf{y}}(\mathbf{u}_{\mathrm{I}}^{(0)})) = 0 \qquad \text{in} \quad \Omega_{\mathrm{I}} \tag{77}$$

$$\nabla_{\mathbf{y}}\cdot(\mathbb{C}_{\mathrm{II}}\xi_{\mathbf{y}}(\mathbf{u}_{\mathrm{II}}^{(0)})) = 0 \qquad \text{in} \quad \Omega_{\mathrm{II}} \tag{78}$$

$$\nabla_{\mathbf{y}}p^{(0)} = 0 \qquad \text{in} \quad \Omega_{\mathrm{f}} \tag{79}$$

We will now equate the coefficients of ϵ^1 in Eqs. (51)–(58) which gives

$$\nabla_{\mathbf{y}}\cdot\boldsymbol{\sigma}_{\mathrm{I}}^{(1)} + \nabla_{\mathbf{x}}\cdot\boldsymbol{\sigma}_{\mathrm{I}}^{(0)} = 0 \quad \text{in} \quad \Omega_{\mathrm{I}} \tag{80}$$

$$\nabla_{\mathbf{y}}\cdot\boldsymbol{\sigma}_{\mathrm{II}}^{(1)} + \nabla_{\mathbf{x}}\cdot\boldsymbol{\sigma}_{\mathrm{II}}^{(0)} = 0 \quad \text{in} \quad \Omega_{\mathrm{II}} \tag{81}$$

$$\nabla_{\mathbf{y}}\cdot\boldsymbol{\sigma}_{\mathrm{f}}^{(1)} + \nabla_{\mathbf{x}}\cdot\boldsymbol{\sigma}_{\mathrm{f}}^{(0)} = 0 \quad \text{in} \quad \Omega_{\mathrm{f}} \tag{82}$$

$$\nabla_{\mathbf{y}}\cdot\mathbf{v}^{(1)} + \nabla_{\mathbf{x}}\cdot\mathbf{v}^{(0)} = 0 \quad \text{in} \quad \Omega_{\mathrm{f}} \tag{83}$$

$$\dot{\mathbf{u}}_{\mathrm{I}}^{(1)} = \mathbf{v}^{(1)} \quad \text{on} \quad \Gamma_{\mathrm{I}} \tag{84}$$

$$\dot{\mathbf{u}}_{\mathrm{II}}^{(1)} = \mathbf{v}^{(1)} \quad \text{on} \quad \Gamma_{\mathrm{II}} \tag{85}$$

$$\boldsymbol{\sigma}_{\mathrm{f}}^{(1)}\mathbf{n}_{\mathrm{I}} = \boldsymbol{\sigma}_{\mathrm{I}}^{(1)}\mathbf{n}_{\mathrm{I}} \quad \text{on} \quad \Gamma_{\mathrm{I}} \tag{86}$$

$$\boldsymbol{\sigma}_{\mathrm{f}}^{(1)}\mathbf{n}_{\mathrm{II}} = \boldsymbol{\sigma}_{\mathrm{II}}^{(1)}\mathbf{n}_{\mathrm{II}} \quad \text{on} \quad \Gamma_{\mathrm{II}} \tag{87}$$

The constitutive equations given by (59)–(61) have coefficients of ϵ^1

$$\boldsymbol{\sigma}_{\mathrm{f}}^{(1)} = -p^{(1)}\mathrm{I} + \xi_{\mathbf{y}}(\mathbf{v}^{(0)}) \quad \text{in} \quad \Omega_{\mathrm{f}} \tag{88}$$

$$\boldsymbol{\sigma}_{\mathrm{I}}^{(0)} = \mathbb{C}_{\mathrm{I}}\xi_{\mathbf{y}}(\mathbf{u}_{\mathrm{I}}^{(1)}) + \mathbb{C}_{\mathrm{I}}\xi_{\mathbf{x}}(\mathbf{u}_{\mathrm{I}}^{(0)}) \quad \text{in} \quad \Omega_{\mathrm{I}} \tag{89}$$

$$\boldsymbol{\sigma}_{\mathrm{II}}^{(0)} = \mathbb{C}_{\mathrm{II}}\xi_{\mathbf{y}}(\mathbf{u}_{\mathrm{II}}^{(1)}) + \mathbb{C}_{\mathrm{II}}\xi_{\mathbf{x}}(\mathbf{u}_{\mathrm{II}}^{(0)}) \quad \text{in} \quad \Omega_{\mathrm{II}} \tag{90}$$

and therefore the balance Eqs. (62)–(64) have coefficients of ϵ^1

$$\begin{aligned}&\nabla_{\mathbf{y}}\cdot(\mathbb{C}_{\mathrm{I}}\xi_{\mathbf{y}}(\mathbf{u}_{\mathrm{I}}^{(1)})) + \nabla_{\mathbf{y}}\cdot(\mathbb{C}_{\mathrm{I}}\xi_{\mathbf{x}}(\mathbf{u}_{\mathrm{I}}^{(0)})) \\ &+ \nabla_{\mathbf{x}}\cdot(\mathbb{C}_{\mathrm{I}}\xi_{\mathbf{y}}(\mathbf{u}_{\mathrm{I}}^{(0)})) = 0 \qquad \text{in} \quad \Omega_{\mathrm{I}},\end{aligned} \tag{91}$$

$$\begin{aligned}&\nabla_{\mathbf{y}}\cdot(\mathbb{C}_{\mathrm{II}}\xi_{\mathbf{y}}(\mathbf{u}_{\mathrm{II}}^{(1)})) + \nabla_{\mathbf{y}}\cdot(\mathbb{C}_{\mathrm{II}}\xi_{\mathbf{x}}(\mathbf{u}_{\mathrm{II}}^{(0)})) \\ &+ \nabla_{\mathbf{x}}\cdot(\mathbb{C}_{\mathrm{II}}\xi_{\mathbf{y}}(\mathbf{u}_{\mathrm{II}}^{(0)})) = 0 \qquad \text{in} \quad \Omega_{\mathrm{II}},\end{aligned} \tag{92}$$

$$\nabla_{\mathbf{y}}^2\mathbf{v}^{(0)} = \nabla_{\mathbf{y}}p^{(1)} + \nabla_{\mathbf{x}}p^{(0)} \qquad \text{in} \quad \Omega_{\mathrm{f}}. \tag{93}$$

From (68) and (74) we can see that that $p^{(0)}$ is independent of the microscale variable $\mathbf{y}$. That is

$$p^{(0)} = p^{(0)}(\mathbf{x}, t). \tag{94}$$

From (75) and (76) we can see that $\mathbf{u}_{\mathrm{I}}^{(0)}$ and $\mathbf{u}_{\mathrm{II}}^{(0)}$ are rigid body motions and therefore this means that by $\mathbf{y}$-periodicity, they do not depend on the microscale variable $\mathbf{y}$. That is

$$\mathbf{u}_{\mathrm{I}}^{(0)} = \mathbf{u}_{\mathrm{I}}^{(0)}(\mathbf{x}, t) \tag{95}$$

$$\mathbf{u}_{\mathrm{II}}^{(0)} = \mathbf{u}_{\mathrm{II}}^{(0)}(\mathbf{x}, t). \tag{96}$$

are the macroscale solid displacements of both the inclusion and the matrix respectively. We will use these throughout the following sections.

3.4. The macroscale fluid flow

We now wish to investigate the leading order of the velocity which we denoted $\mathbf{v}^{(0)}$.

Traditionally in works of this kind, at this point we would introduce a single relative fluid–solid velocity, see Burridge and Keller (1981), Penta et al. (2014), Miller and Penta (2020), Penta et al. (2020), Miller and Penta (2021b, 2023a) and Miller and Penta (2023b). This however relies on the continuity of the leading order solid velocities $\mathbf{u}_{\mathrm{I}}^{(0)}$ and $\dot{\mathbf{u}}_{\mathrm{II}}^{(0)}$. This does not apply in this work since we have a complete decoupling of the two solid phases. This would mean that we would either have to introduce two relative fluid–solid velocities or indeed progress using the absolute velocity $\mathbf{v}^{(0)}$.

Using Eqs. (70), (71), (74), (82) and (88), we have a Stokes'-type boundary value problem which is given by

$$\nabla_{\mathbf{y}}^2\mathbf{v}^{(0)} - \nabla_{\mathbf{y}}p^{(1)} - \nabla_{\mathbf{x}}p^{(0)} = 0 \qquad \text{in} \quad \Omega_{\mathrm{f}} \tag{97}$$

$$\nabla_{\mathbf{y}}\cdot\mathbf{v}^{(0)} = 0 \qquad \text{in} \quad \Omega_{\mathrm{f}} \tag{98}$$

$$\mathbf{v}^{(0)} = \dot{\mathbf{u}}_{\mathrm{I}}^{(0)} \qquad \text{on} \quad \Gamma_{\mathrm{I}} \tag{99}$$

$$\mathbf{v}^{(0)} = \dot{\mathbf{u}}_{\mathrm{II}}^{(0)} \qquad \text{on} \quad \Gamma_{\mathrm{II}} \tag{100}$$

By exploiting linearity and using (94) we suggest the following ansatz for the problem (97)–(100),

$$\mathbf{v}^{(0)} = -\mathsf{W}\nabla_{\mathbf{x}}p^{(0)} + \mathsf{G}\dot{\mathbf{u}}_{\mathrm{I}}^{(0)} + \mathsf{L}\dot{\mathbf{u}}_{\mathrm{II}}^{(0)}, \tag{101}$$

$$p^{(1)} = -\mathbf{P}\cdot\nabla_{\mathbf{x}}p^{(0)} + \mathbf{H}\cdot\dot{\mathbf{u}}_{\mathrm{I}}^{(0)} + \mathbf{S}\cdot\dot{\mathbf{u}}_{\mathrm{II}}^{(0)} + c(\mathbf{x}), \tag{102}$$

Eqs. (101) and (102) are the solution to the problem (97)–(100) provided that second rank tensors W, G, L and vectors $\mathbf{P}$, $\mathbf{H}$ and $\mathbf{S}$ satisfy the following cell problems

$$\begin{cases} \nabla_{\mathbf{y}}^2\mathsf{W}^{\mathrm{T}} - \nabla_{\mathbf{y}}\mathbf{P} + \mathrm{I} = 0 & \text{in} \quad \Omega_{\mathrm{f}} \\ \nabla_{\mathbf{y}}\cdot\mathsf{W}^{\mathrm{T}} = 0 & \text{in} \quad \Omega_{\mathrm{f}} \\ \mathsf{W}^{\mathrm{T}} = 0 & \text{on} \quad \Gamma_{\mathrm{I}} \\ \mathsf{W}^{\mathrm{T}} = 0 & \text{on} \quad \Gamma_{\mathrm{II}}, \end{cases} \tag{103}$$

and

$$\begin{cases} \nabla_{\mathbf{y}}^2\mathsf{G}^{\mathrm{T}} = \nabla_{\mathbf{y}}\mathbf{H} & \text{in} \quad \Omega_{\mathrm{f}} \\ \nabla_{\mathbf{y}}\cdot\mathsf{G}^{\mathrm{T}} = 0 & \text{in} \quad \Omega_{\mathrm{f}} \\ \mathsf{G}^{\mathrm{T}} = \mathrm{I} & \text{on} \quad \Gamma_{\mathrm{I}} \\ \mathsf{G}^{\mathrm{T}} = 0 & \text{on} \quad \Gamma_{\mathrm{II}}, \end{cases} \tag{104}$$

and

$$\begin{cases} \nabla_{\mathbf{y}}^2\mathsf{L}^{\mathrm{T}} = \nabla_{\mathbf{y}}\mathbf{S} & \text{in} \quad \Omega_{\mathrm{f}} \\ \nabla_{\mathbf{y}}\cdot\mathsf{L}^{\mathrm{T}} = 0 & \text{in} \quad \Omega_{\mathrm{f}} \\ \mathsf{L}^{\mathrm{T}} = 0 & \text{on} \quad \Gamma_{\mathrm{I}} \\ \mathsf{L}^{\mathrm{T}} = \mathrm{I} & \text{on} \quad \Gamma_{\mathrm{II}}, \end{cases} \tag{105}$$

where periodic conditions apply on the boundary $\partial\Omega_{\mathrm{f}}\setminus\Gamma_{\mathrm{I}}\cup\Gamma_{\mathrm{II}}$ and a further condition is to be placed on $\mathbf{P}$, $\mathbf{H}$ and $\mathbf{S}$ for the solution to be unique (for example zero average on the fluid cell portion).

Remark 4 (*Fluid Cell Problems*)**.** The novel fluid cell problems (103)–(105) incorporate how the fluid flows through gap between the matrix and the fibre network. These include the fact that the fluid flow is interacting with both of the elastic phases and has a continuity between the fluid velocity and the solid velocity of both phases on the interfaces between the phases yet accounts for the fact that there is no continuity between the two elastic phases.

Taking the integral average of (101) over the fluid domain leads to

$$\langle\mathbf{v}^{(0)}\rangle_{\mathrm{f}} = -\langle\mathsf{W}\rangle_{\mathrm{f}}\nabla_{\mathbf{x}}p^{(0)} + \langle\mathsf{G}\rangle_{\mathrm{f}}\dot{\mathbf{u}}_{\mathrm{I}}^{(0)} + \langle\mathsf{L}\rangle_{\mathrm{f}}\dot{\mathbf{u}}_{\mathrm{II}}^{(0)}, \tag{106}$$

which governs the fluid on the macroscale.

3.5. Macroscale poroelasticity

In order to close the system for the elastic displacement $\mathbf{u}_{\mathrm{I}}^{(0)}$, $\mathbf{u}_{\mathrm{II}}^{(0)}$ and $p^{(0)}$ we require macroscale governing equations. We take the integral averages of Eq. (80) to obtain

$$\int_{\Omega_{\mathrm{I}}}\nabla_{\mathbf{y}}\cdot\boldsymbol{\sigma}_{\mathrm{I}}^{(1)}\mathrm{d}\mathbf{y} + \int_{\Omega_{\mathrm{I}}}\nabla_{\mathbf{x}}\cdot\boldsymbol{\sigma}_{\mathrm{I}}^{(0)}\mathrm{d}\mathbf{y} = 0. \tag{107}$$

We then apply Gauss' divergence theorem to the first integral and apply macroscopic uniformity to the second. This means we obtain

$$\int_{\partial\Omega_{\mathrm{I}}\setminus\Gamma_{\mathrm{I}}}\boldsymbol{\sigma}_{\mathrm{I}}^{(1)}\mathbf{n}_{\Omega_{\mathrm{I}}\setminus\Gamma_{\mathrm{I}}}\,\mathrm{dS} + \int_{\Gamma_{\mathrm{I}}}\boldsymbol{\sigma}_{\mathrm{I}}^{(1)}\mathbf{n}_{\mathrm{I}}\,\mathrm{dS} + \nabla_{\mathbf{x}}\cdot\int_{\Omega_{\mathrm{I}}}\boldsymbol{\sigma}_{\mathrm{I}}^{(0)}\mathrm{d}\mathbf{y} = 0, \tag{108}$$

where we have that $\mathbf{n}_{\mathrm{I}}$ and $\mathbf{n}_{\Omega_{\mathrm{I}}\setminus\Gamma_{\mathrm{I}}}$ are the unit normals corresponding to Γ_{I} and $\partial\Omega_{\mathrm{I}}\setminus\Gamma_{\mathrm{I}}$. The contributions over the external boundaries of the phase Ω_{I} will cancel due to $\mathbf{y}$-periodicity. Therefore (108) becomes

$$\int_{\Gamma_{\mathrm{I}}}\boldsymbol{\sigma}_{\mathrm{I}}^{(1)}\mathbf{n}_{\mathrm{I}}\,\mathrm{dS} + \nabla_{\mathbf{x}}\cdot\int_{\Omega_{\mathrm{I}}}\boldsymbol{\sigma}_{\mathrm{I}}^{(0)}\mathrm{d}\mathbf{y} = 0. \tag{109}$$

By using the interface condition (86) we can write

$$\int_{\Gamma_{\mathrm{I}}}\boldsymbol{\sigma}_{\mathrm{f}}^{(1)}\mathbf{n}_{\mathrm{I}}\,\mathrm{dS} + \nabla_{\mathbf{x}}\cdot\int_{\Omega_{\mathrm{I}}}\boldsymbol{\sigma}_{\mathrm{I}}^{(0)}\mathrm{d}\mathbf{y} = 0. \tag{110}$$

We are then able to use the expression (88) for $\boldsymbol{\sigma}_{\mathrm{f}}^{(1)}$ and substitute in the first integral to obtain

$$\int_{\Gamma_{\mathrm{I}}}\left(-p^{(1)}\mathrm{I} + \xi_{\mathbf{y}}(\mathbf{v}^{(0)})\right)\mathbf{n}_{\mathrm{I}}\,\mathrm{dS} + \nabla_{\mathbf{x}}\cdot\int_{\Omega_{\mathrm{I}}}\boldsymbol{\sigma}_{\mathrm{I}}^{(0)}\mathrm{d}\mathbf{y} = 0. \tag{111}$$

We can then use the expression (101) and (102) for $\mathbf{v}^{(0)}$ and $p^{(1)}$ to rewrite (111) as

$$\begin{aligned}&\int_{\Gamma_{\mathrm{I}}}\left(\mathbf{P}\cdot\nabla_{\mathbf{x}}p^{(0)} - \mathbf{H}\cdot\dot{\mathbf{u}}_{\mathrm{I}}^{(0)} - \mathbf{S}\cdot\dot{\mathbf{u}}_{\mathrm{II}}^{(0)} + c(\mathbf{x})\right)\mathbf{n}_{\mathrm{I}}\,\mathrm{dS}\\ &+\int_{\Gamma_{\mathrm{I}}}\left(-\xi_{\mathbf{y}}(\mathsf{W})\nabla_{\mathbf{x}}p^{(0)} + \xi_{\mathbf{y}}(\mathsf{G})\dot{\mathbf{u}}_{\mathrm{I}}^{(0)} + \xi_{\mathbf{y}}(\mathsf{L})\dot{\mathbf{u}}_{\mathrm{II}}^{(0)}\right)\mathbf{n}_{\mathrm{I}}\,\mathrm{dS}\\ &+\nabla_{\mathbf{x}}\cdot\int_{\Omega_{\mathrm{I}}}\boldsymbol{\sigma}_{\mathrm{I}}^{(0)}\mathrm{d}\mathbf{y} = 0.\end{aligned} \tag{112}$$

Since the terms $\nabla_{\mathbf{x}}p^{(0)}$, $\dot{\mathbf{u}}_{\mathrm{I}}^{(0)}$ and $\dot{\mathbf{u}}_{\mathrm{II}}^{(0)}$ do not depend on the microscale variable $\mathbf{y}$ we can remove these terms from the integral. That is

$$\begin{aligned}&\left(\int_{\Gamma_{\mathrm{I}}}\mathbf{n}_{\mathrm{I}}\otimes\mathbf{P}\,\mathrm{dS} - \int_{\Gamma_{\mathrm{I}}}\xi_{\mathbf{y}}(\mathsf{W})\mathbf{n}_{\mathrm{I}}\,\mathrm{dS}\right)\nabla_{\mathbf{x}}p^{(0)}\\ &+\left(\int_{\Gamma_{\mathrm{I}}}\xi_{\mathbf{y}}(\mathsf{G})\mathbf{n}_{\mathrm{I}}\,\mathrm{dS} - \int_{\Gamma_{\mathrm{I}}}\mathbf{n}_{\mathrm{I}}\otimes\mathbf{H}\,\mathrm{dS}\right)\dot{\mathbf{u}}_{\mathrm{I}}^{(0)}\\ &+\left(\int_{\Gamma_{\mathrm{I}}}\xi_{\mathbf{y}}(\mathsf{L})\mathbf{n}_{\mathrm{I}}\,\mathrm{dS} - \int_{\Gamma_{\mathrm{I}}}\mathbf{n}_{\mathrm{I}}\otimes\mathbf{S}\,\mathrm{dS}\right)\dot{\mathbf{u}}_{\mathrm{II}}^{(0)}\\ &+c(\mathbf{x})\int_{\Gamma_{\mathrm{I}}}\mathbf{n}_{\mathrm{I}}\,\mathrm{dS} + \nabla_{\mathbf{x}}\cdot\int_{\Omega_{\mathrm{I}}}\boldsymbol{\sigma}_{\mathrm{I}}^{(0)}\mathrm{d}\mathbf{y} = 0.\end{aligned} \tag{113}$$

Where due to wishing to factorize the term $\nabla_{\mathbf{x}}p^{(0)}$ out of the first term in (112), $\mathbf{P}\nabla_{\mathbf{x}}p^{(0)}\mathbf{n}_{\mathrm{I}}$ we make use of the tensor/outer product between the two vectors $\mathbf{n}_{\mathrm{I}}$ and $\mathbf{P}$, which we write as $\mathbf{n}_{\mathrm{I}}\otimes\mathbf{P}$ and in components $n_i^{\mathrm{I}}P_j$. The same principle is applied to the second and third terms in (112) to factor out $\dot{\mathbf{u}}_{\mathrm{I}}^{(0)}$ and $\dot{\mathbf{u}}_{\mathrm{II}}^{(0)}$ respectively. By reversing the divergence theorem on the second from last integral it disappears and the final balance equation for the material including surface integrals can be written as

$$\begin{aligned}&\nabla_{\mathbf{x}}\cdot\langle\boldsymbol{\sigma}_{\mathrm{I}}^{(0)}\rangle_{\mathrm{I}} + \left(\int_{\Gamma_{\mathrm{I}}}\mathbf{n}_{\mathrm{I}}\otimes\mathbf{P}\,\mathrm{dS} - \int_{\Gamma_{\mathrm{I}}}\xi_{\mathbf{y}}(\mathsf{W})\mathbf{n}_{\mathrm{I}}\,\mathrm{dS}\right)\nabla_{\mathbf{x}}p^{(0)}\\ &+\left(\int_{\Gamma_{\mathrm{I}}}\xi_{\mathbf{y}}(\mathsf{G})\mathbf{n}_{\mathrm{I}}\,\mathrm{dS} - \int_{\Gamma_{\mathrm{I}}}\mathbf{n}_{\mathrm{I}}\otimes\mathbf{H}\,\mathrm{dS}\right)\dot{\mathbf{u}}_{\mathrm{I}}^{(0)}\\ &+\left(\int_{\Gamma_{\mathrm{I}}}\xi_{\mathbf{y}}(\mathsf{L})\mathbf{n}_{\mathrm{I}}\,\mathrm{dS} - \int_{\Gamma_{\mathrm{I}}}\mathbf{n}_{\mathrm{I}}\otimes\mathbf{S}\,\mathrm{dS}\right)\dot{\mathbf{u}}_{\mathrm{II}}^{(0)} = 0.\end{aligned} \tag{114}$$

We can also perform similar calculations for the stress-balance of the matrix portion of the cell. We take the integral average (81) to obtain

$$\int_{\Omega_{\mathrm{II}}} \nabla_{\mathbf{y}} \cdot \boldsymbol{\sigma}_{\mathrm{II}}^{(1)} \mathrm{d}\mathbf{y} + \int_{\Omega_{\mathrm{II}}} \nabla_{\mathbf{x}} \cdot \boldsymbol{\sigma}_{\mathrm{II}}^{(0)} \mathrm{d}\mathbf{y} = 0. \tag{115}$$

We then apply Gauss' divergence theorem to the first integral and apply macroscopic uniformity to the second. This means we obtain

$$\int_{\partial\Omega_{\mathrm{II}} \setminus \Gamma_{\mathrm{II}}} \boldsymbol{\sigma}_{\mathrm{II}}^{(1)} \mathbf{n}_{\Omega_{\mathrm{II}} \setminus \Gamma_{\mathrm{II}}} \, \mathrm{dS} + \int_{\Gamma_{\mathrm{II}}} \boldsymbol{\sigma}_{\mathrm{II}}^{(1)} \mathbf{n}_{\mathrm{II}} \, \mathrm{dS} + \nabla_{\mathbf{x}} \cdot \int_{\Omega_{\mathrm{II}}} \boldsymbol{\sigma}_{\mathrm{II}}^{(0)} \mathrm{d}\mathbf{y} = 0, \tag{116}$$

where we have that $\mathbf{n}_{\mathrm{II}}$ and $\mathbf{n}_{\Omega_{\mathrm{II}} \setminus \Gamma_{\mathrm{II}}}$ are the unit normals corresponding to Γ_{II} and $\partial\Omega_{\mathrm{II}} \setminus \Gamma_{\mathrm{II}}$. The contributions over the external boundaries of the phase Ω_{II} will cancel due to $\mathbf{y}$-periodicity. Therefore (116) becomes

$$\int_{\Gamma_{\mathrm{II}}} \boldsymbol{\sigma}_{\mathrm{II}}^{(1)} \mathbf{n}_{\mathrm{II}} \, \mathrm{dS} + \nabla_{\mathbf{x}} \cdot \int_{\Omega_{\mathrm{II}}} \boldsymbol{\sigma}_{\mathrm{II}}^{(0)} \mathrm{d}\mathbf{y} = 0. \tag{117}$$

By using the interface condition (87) we can write

$$\int_{\Gamma_{\mathrm{II}}} \boldsymbol{\sigma}_{\mathrm{f}}^{(1)} \mathbf{n}_{\mathrm{II}} \, \mathrm{dS} + \nabla_{\mathbf{x}} \cdot \int_{\Omega_{\mathrm{II}}} \boldsymbol{\sigma}_{\mathrm{II}}^{(0)} \mathrm{d}\mathbf{y} = 0. \tag{118}$$

We are then able to use the expression (88) for $\boldsymbol{\sigma}_{\mathrm{f}}^{(1)}$ and substitute in the first integral to obtain

$$\int_{\Gamma_{\mathrm{II}}} (-p^{(1)}\mathbf{I} + \xi_{\mathbf{y}}(\mathbf{v}^{(0)})) \mathbf{n}_{\mathrm{II}} \, \mathrm{dS} + \nabla_{\mathbf{x}} \cdot \int_{\Omega_{\mathrm{II}}} \boldsymbol{\sigma}_{\mathrm{II}}^{(0)} \mathrm{d}\mathbf{y} = 0. \tag{119}$$

We can then use the expression (101) and (102) for $\mathbf{v}^{(0)}$ and $p^{(1)}$ to rewrite (119) as

$$\begin{aligned} &\int_{\Gamma_{\mathrm{II}}} \left(\mathbf{P} \cdot \nabla_{\mathbf{x}} p^{(0)} - \mathbf{H} \cdot \dot{\mathbf{u}}_{\mathrm{I}}^{(0)} - \mathbf{S} \cdot \dot{\mathbf{u}}_{\mathrm{II}}^{(0)} + c(\mathbf{x}) \right) \mathbf{n}_{\mathrm{II}} \, \mathrm{dS} \\ &+ \int_{\Gamma_{\mathrm{II}}} \left(-\xi_{\mathbf{y}}(\mathsf{W}) \nabla_{\mathbf{x}} p^{(0)} + \xi_{\mathbf{y}}(\mathsf{G}) \dot{\mathbf{u}}_{\mathrm{I}}^{(0)} + \xi_{\mathbf{y}}(\mathsf{L}) \dot{\mathbf{u}}_{\mathrm{II}}^{(0)} \right) \mathbf{n}_{\mathrm{II}} \, \mathrm{dS} \\ &+ \nabla_{\mathbf{x}} \cdot \int_{\Omega_{\mathrm{II}}} \boldsymbol{\sigma}_{\mathrm{II}}^{(0)} \mathrm{d}\mathbf{y} = 0. \end{aligned} \tag{120}$$

Since the terms $\nabla_{\mathbf{x}} p^{(0)}$, $\dot{\mathbf{u}}_{\mathrm{I}}^{(0)}$ and $\dot{\mathbf{u}}_{\mathrm{II}}^{(0)}$ do not depend on the microscale variable $\mathbf{y}$ we can remove these terms from the integral. That is

$$\begin{aligned} &\left(\int_{\Gamma_{\mathrm{II}}} \mathbf{n}_{\mathrm{II}} \otimes \mathbf{P} \, \mathrm{dS} - \int_{\Gamma_{\mathrm{II}}} \xi_{\mathbf{y}}(\mathsf{W}) \mathbf{n}_{\mathrm{II}} \, \mathrm{dS} \right) \nabla_{\mathbf{x}} p^{(0)} \\ &+ \left(\int_{\Gamma_{\mathrm{II}}} \xi_{\mathbf{y}}(\mathsf{G}) \mathbf{n}_{\mathrm{II}} \, \mathrm{dS} - \int_{\Gamma_{\mathrm{II}}} \mathbf{n}_{\mathrm{II}} \otimes \mathbf{H} \, \mathrm{dS} \right) \dot{\mathbf{u}}_{\mathrm{I}}^{(0)} \\ &+ \left(\int_{\Gamma_{\mathrm{II}}} \xi_{\mathbf{y}}(\mathsf{L}) \mathbf{n}_{\mathrm{II}} \, \mathrm{dS} - \int_{\Gamma_{\mathrm{II}}} \mathbf{n}_{\mathrm{II}} \otimes \mathbf{S} \, \mathrm{dS} \right) \dot{\mathbf{u}}_{\mathrm{II}}^{(0)} \\ &+ c(\mathbf{x}) \int_{\Gamma_{\mathrm{II}}} \mathbf{n}_{\mathrm{II}} \, \mathrm{dS} + \nabla_{\mathbf{x}} \cdot \int_{\Omega_{\mathrm{II}}} \boldsymbol{\sigma}_{\mathrm{II}}^{(0)} \mathrm{d}\mathbf{y} = 0. \end{aligned} \tag{121}$$

Where due to wishing to factorize the term $\nabla_{\mathbf{x}} p^{(0)}$ out of the first term in (120), $\mathbf{P} \nabla_{\mathbf{x}} p^{(0)} \mathbf{n}_{\mathrm{II}}$, we make use of the tensor/outer product between the two vectors $\mathbf{n}_{\mathrm{II}}$ and $\mathbf{P}$, which we write as $\mathbf{n}_{\mathrm{II}} \otimes \mathbf{P}$ and in components $n_i^{\mathrm{II}} P_j$. The same principle is applied to the second and third terms in (120) to factor out $\dot{\mathbf{u}}_{\mathrm{I}}^{(0)}$ and $\dot{\mathbf{u}}_{\mathrm{II}}^{(0)}$ respectively. Then finally by reversing the divergence theorem on the second from last integral it disappears and the final balance equation for the material including surface integrals can be written as

$$\begin{aligned} &\nabla_{\mathbf{x}} \cdot \langle \boldsymbol{\sigma}_{\mathrm{II}}^{(0)} \rangle_{\mathrm{II}} \\ &+ \left(\int_{\Gamma_{\mathrm{II}}} \mathbf{n}_{\mathrm{II}} \otimes \mathbf{P} \, \mathrm{dS} - \int_{\Gamma_{\mathrm{II}}} \xi_{\mathbf{y}}(\mathsf{W}) \mathbf{n}_{\mathrm{II}} \, \mathrm{dS} \right) \nabla_{\mathbf{x}} p^{(0)} \\ &+ \left(\int_{\Gamma_{\mathrm{II}}} \xi_{\mathbf{y}}(\mathsf{G}) \mathbf{n}_{\mathrm{II}} \, \mathrm{dS} - \int_{\Gamma_{\mathrm{II}}} \mathbf{n}_{\mathrm{II}} \otimes \mathbf{H} \, \mathrm{dS} \right) \dot{\mathbf{u}}_{\mathrm{I}}^{(0)} \\ &+ \left(\int_{\Gamma_{\mathrm{II}}} \xi_{\mathbf{y}}(\mathsf{L}) \mathbf{n}_{\mathrm{II}} \, \mathrm{dS} - \int_{\Gamma_{\mathrm{II}}} \mathbf{n}_{\mathrm{II}} \otimes \mathbf{S} \, \mathrm{dS} \right) \dot{\mathbf{u}}_{\mathrm{II}}^{(0)} = 0. \end{aligned} \tag{122}$$

We therefore have two balance Eqs. (114) and (122), one for each solid domain respectively.

By using Eqs. (66), (67), (72)–(74), (89) and (90) and exploiting (94) we can write the following problems for $\mathbf{u}_{\mathrm{I}}^{(0)}$ and $\mathbf{u}_{\mathrm{II}}^{(0)}$

$$\nabla_{\mathbf{y}} \cdot (\mathbb{C}_{\mathrm{I}} \xi_{\mathbf{y}}(\mathbf{u}_{\mathrm{I}}^{(1)})) + \nabla_{\mathbf{y}} \cdot (\mathbb{C}_{\mathrm{I}} \xi_{\mathbf{x}}(\mathbf{u}_{\mathrm{I}}^{(0)})) = 0 \quad \text{in} \quad \Omega_{\mathrm{I}} \tag{123}$$

$$(\mathbb{C}_{\mathrm{I}} \xi_{\mathbf{y}}(\mathbf{u}_{\mathrm{I}}^{(1)}) + \mathbb{C}_{\mathrm{I}} \xi_{\mathbf{x}}(\mathbf{u}_{\mathrm{I}}^{(0)})) \mathbf{n}_{\mathrm{I}} = -p^{(0)} \mathbf{n}_{\mathrm{I}} \quad \text{on} \quad \Gamma_{\mathrm{I}} \tag{124}$$

and

$$\nabla_{\mathbf{y}} \cdot (\mathbb{C}_{\mathrm{II}} \xi_{\mathbf{y}}(\mathbf{u}_{\mathrm{II}}^{(1)})) + \nabla_{\mathbf{y}} \cdot (\mathbb{C}_{\mathrm{II}} \xi_{\mathbf{x}}(\mathbf{u}_{\mathrm{II}}^{(0)})) = 0 \quad \text{in} \quad \Omega_{\mathrm{II}} \tag{125}$$

$$(\mathbb{C}_{\mathrm{II}} \xi_{\mathbf{y}}(\mathbf{u}_{\mathrm{II}}^{(1)}) + \mathbb{C}_{\mathrm{II}} \xi_{\mathbf{x}}(\mathbf{u}_{\mathrm{II}}^{(0)})) \mathbf{n}_{\mathrm{II}} = -p^{(0)} \mathbf{n}_{\mathrm{II}} \quad \text{on} \quad \Gamma_{\mathrm{II}} \tag{126}$$

The solutions to the problems given by (123)–(124) and (125)–(126), exploiting linearity are

$$\mathbf{u}_{\mathrm{I}}^{(1)} = A_{\mathrm{I}} \xi_{\mathbf{x}}(\mathbf{u}_{\mathrm{I}}^{(0)}) + \mathbf{a}_{\mathrm{I}} p^{(0)} \tag{127}$$

$$\mathbf{u}_{\mathrm{II}}^{(1)} = A_{\mathrm{II}} \xi_{\mathbf{x}}(\mathbf{u}_{\mathrm{II}}^{(0)}) + \mathbf{a}_{\mathrm{II}} p^{(0)} \tag{128}$$

respectively, where we have that A_{I} and A_{II} are third rank tensors and $\mathbf{a}_{\mathrm{I}}$ and $\mathbf{a}_{\mathrm{II}}$ are vectors. The following cell problems are to be satisfied by A_{I}, A_{II}, $\mathbf{a}_{\mathrm{I}}$ and $\mathbf{a}_{\mathrm{II}}$. The cell problems are

$$\nabla_{\mathbf{y}} \cdot (\mathbb{C}_{\mathrm{I}} \xi_{\mathbf{y}}(A_{\mathrm{I}})) + \nabla_{\mathbf{y}} \cdot \mathbb{C}_{\mathrm{I}} = 0 \qquad \text{in} \quad \Omega_{\mathrm{I}} \tag{129}$$

$$(\mathbb{C}_{\mathrm{I}} \xi_{\mathbf{y}}(A_{\mathrm{I}})) \mathbf{n}_{\mathrm{I}} + \mathbb{C}_{\mathrm{I}} \mathbf{n}_{\mathrm{I}} = 0 \qquad \text{on} \quad \Gamma_{\mathrm{I}} \tag{130}$$

and

$$\nabla_{\mathbf{y}} \cdot (\mathbb{C}_{\mathrm{II}} \xi_{\mathbf{y}}(A_{\mathrm{II}})) + \nabla_{\mathbf{y}} \cdot \mathbb{C}_{\mathrm{II}} = 0 \qquad \text{in} \quad \Omega_{\mathrm{II}} \tag{131}$$

$$(\mathbb{C}_{\mathrm{II}} \xi_{\mathbf{y}}(A_{\mathrm{II}})) \mathbf{n}_{\mathrm{II}} + \mathbb{C}_{\mathrm{II}} \mathbf{n}_{\mathrm{II}} = 0 \qquad \text{on} \quad \Gamma_{\mathrm{II}} \tag{132}$$

and

$$\nabla_{\mathbf{y}} \cdot (\mathbb{C}_{\mathrm{I}} \xi_{\mathbf{y}}(\mathbf{a}_{\mathrm{I}})) = 0 \qquad \text{in} \quad \Omega_{\mathrm{I}} \tag{133}$$

$$(\mathbb{C}_{\mathrm{I}} \xi_{\mathbf{y}}(\mathbf{a}_{\mathrm{I}})) \mathbf{n}_{\mathrm{I}} + \mathbf{n}_{\mathrm{I}} = 0 \qquad \text{on} \quad \Gamma_{\mathrm{I}} \tag{134}$$

and

$$\nabla_{\mathbf{y}} \cdot (\mathbb{C}_{\mathrm{II}} \xi_{\mathbf{y}}(\mathbf{a}_{\mathrm{II}})) = 0 \qquad \text{in} \quad \Omega_{\mathrm{II}} \tag{135}$$

$$(\mathbb{C}_{\mathrm{II}} \xi_{\mathbf{y}}(\mathbf{a}_{\mathrm{II}})) \mathbf{n}_{\mathrm{II}} + \mathbf{n}_{\mathrm{II}} = 0 \qquad \text{on} \quad \Gamma_{\mathrm{II}} \tag{136}$$

These cell problems are to be supplemented by periodic conditions on the boundaries $\partial\Omega_{\mathrm{II}} \setminus \Gamma_{\mathrm{II}}$ and $\partial\Omega_{\mathrm{I}} \setminus \Gamma_{\mathrm{I}}$, and for the uniqueness of the solutions, further conditions on the auxiliary variables A_{I}, A_{II}, $\mathbf{a}_{\mathrm{I}}$ and $\mathbf{a}_{\mathrm{II}}$ is required i.e.

$$\begin{aligned} &\langle A_{\mathrm{I}} \rangle_{\mathrm{I}} = 0, \quad \langle A_{\mathrm{II}} \rangle_{\mathrm{II}} = 0, \\ &\langle \mathbf{a}_{\mathrm{I}} \rangle_{\mathrm{I}} = 0, \quad \langle \mathbf{a}_{\mathrm{II}} \rangle_{\mathrm{II}} = 0. \end{aligned} \tag{137}$$

Remark 5 (*Elastic Cell Problems*)**.** We have presented four cell problems (129)–(130), (131)–(132), (133)–(134) and (135)–(136) that can be solved to find the coefficients of the final model. We should note that the cell problems for the two elastic phases are completely decoupled and can be seen to be two sets (129)–(130) and (133)–(134) for the fibre network and (131)–(132) and (135)–(136) for the matrix which are the typical cell problems associated with poroelasticity.

We now want an expression for the leading order solid stress tensors. From (89) and (90) we have that $\mathbf{u}_{\mathrm{I}}^{(1)}$ and $\mathbf{u}_{\mathrm{II}}^{(1)}$ are related to the leading order stresses $\boldsymbol{\sigma}_{\mathrm{I}}^{(0)}$ and $\boldsymbol{\sigma}_{\mathrm{II}}^{(0)}$ respectively. This means we can write

$$\boldsymbol{\sigma}_{\mathrm{I}}^{(0)} = \mathbb{C}_{\mathrm{I}} \mathbb{M}_{\mathrm{I}} \xi_{\mathbf{x}}(\mathbf{u}_{\mathrm{I}}^{(0)}) + \mathbb{C}_{\mathrm{I}} Q_{\mathrm{I}} p^{(0)} + \mathbb{C}_{\mathrm{I}} \xi_{\mathbf{x}}(\mathbf{u}_{\mathrm{I}}^{(0)}) \tag{138}$$

and

$$\boldsymbol{\sigma}_{\mathrm{II}}^{(0)} = \mathbb{C}_{\mathrm{II}} \mathbb{M}_{\mathrm{II}} \xi_{\mathbf{x}}(\mathbf{u}_{\mathrm{II}}^{(0)}) + \mathbb{C}_{\mathrm{II}} Q_{\mathrm{II}} p^{(0)} + \mathbb{C}_{\mathrm{II}} \xi_{\mathbf{x}}(\mathbf{u}_{\mathrm{II}}^{(0)}) \tag{139}$$

where we have used that

$$\mathbb{M}_{\mathrm{I}} = \xi_{\mathbf{y}}(A_{\mathrm{I}}) = \xi_{pq}^{kl}(A^{\mathrm{I}}) = \frac{1}{2} \left(\frac{\partial A_{pkl}^{\mathrm{I}}}{\partial y_q} + \frac{\partial A_{qkl}^{\mathrm{I}}}{\partial y_p} \right), \tag{140}$$

$$\mathbb{M}_{\mathrm{II}} = \xi_{\mathbf{y}}(A_{\mathrm{II}}) = \xi^{kl}_{pq}(A^{\mathrm{II}}) = \frac{1}{2}\left(\frac{\partial A^{\mathrm{II}}_{pkl}}{\partial y_q} + \frac{\partial A^{\mathrm{II}}_{qkl}}{\partial y_p}\right), \tag{141}$$

$$Q_{\mathrm{I}} = \xi_{\mathbf{y}}(\mathbf{a}_{\mathrm{I}}) = \xi_{ij}(\mathbf{a}^{\mathrm{I}}) = \frac{1}{2}\left(\frac{\partial \mathbf{a}^{\mathrm{I}}_i}{\partial y_j} + \frac{\partial \mathbf{a}^{\mathrm{I}}_j}{\partial y_i}\right), \tag{142}$$

$$Q_{\mathrm{II}} = \xi_{\mathbf{y}}(\mathbf{a}_{\mathrm{II}}) = \xi_{ij}(\mathbf{a}^{\mathrm{II}}) = \frac{1}{2}\left(\frac{\partial \mathbf{a}^{\mathrm{II}}_i}{\partial y_j} + \frac{\partial \mathbf{a}^{\mathrm{II}}_j}{\partial y_i}\right) \tag{143}$$

We can now take our expressions for the leading order solid stresses, (138) and (139), and taking the integral average over the individual solid domains gives

$$\langle \boldsymbol{\sigma}^{(0)}_{\mathrm{I}} \rangle_{\mathrm{I}} = \langle \mathbb{C}_{\mathrm{I}}\mathbb{M}_{\mathrm{I}} + \mathbb{C}_{\mathrm{I}} \rangle_{\mathrm{I}} \xi_{\mathbf{x}}(\mathbf{u}^{(0)}_{\mathrm{I}}) + \langle \mathbb{C}_{\mathrm{I}} Q_{\mathrm{I}} \rangle_{\mathrm{I}} p^{(0)} \tag{144}$$

$$\langle \boldsymbol{\sigma}^{(0)}_{\mathrm{II}} \rangle_{\mathrm{II}} = \langle \mathbb{C}_{\mathrm{II}}\mathbb{M}_{\mathrm{II}} + \mathbb{C}_{\mathrm{II}} \rangle_{\mathrm{II}} \xi_{\mathbf{x}}(\mathbf{u}^{(0)}_{\mathrm{II}}) + \langle \mathbb{C}_{\mathrm{II}} Q_{\mathrm{II}} \rangle_{\mathrm{II}} p^{(0)} \tag{145}$$

These can be used in (114) and (122) to give the average force balance equations for our poroelastic composite material.

We wish to obtain a conservation of mass equation for our material. To do this we return to Eq. (83), the incompressibility constraint, and we integrate to obtain

$$0 = \int_{\Omega_{\mathrm{f}}} \nabla_{\mathbf{y}} \cdot \mathbf{v}^{(1)} \mathrm{d}\mathbf{y} + \int_{\Omega_{\mathrm{f}}} \nabla_{\mathbf{x}} \cdot \mathbf{v}^{(0)} \mathrm{d}\mathbf{y} \tag{146}$$

Then we apply Gauss' divergence theorem twice to the first integral and use the interface conditions (84) and (85), we also rearrange the second integral to obtain

$$\begin{aligned} 0 &= -\int_{\Omega_{\mathrm{I}}} \nabla_{\mathbf{y}} \cdot \dot{\mathbf{u}}^{(1)}_{\mathrm{I}} \mathrm{d}\mathbf{y} - \int_{\Omega_{\mathrm{II}}} \nabla_{\mathbf{y}} \cdot \dot{\mathbf{u}}^{(1)}_{\mathrm{II}} \mathrm{d}\mathbf{y} + \nabla_{\mathbf{x}} \cdot \langle \mathbf{v}^{(0)} \rangle_{\mathrm{f}} \\ &= -\int_{\Omega_{\mathrm{I}}} \mathrm{Tr}(\xi_{\mathbf{y}}(\dot{\mathbf{u}}^{(1)}_{\mathrm{I}})) \mathrm{d}\mathbf{y} - \int_{\Omega_{\mathrm{II}}} \mathrm{Tr}(\xi_{\mathbf{y}}(\dot{\mathbf{u}}^{(1)}_{\mathrm{II}})) \mathrm{d}\mathbf{y} \\ &\quad + \nabla_{\mathbf{x}} \cdot \langle \mathbf{v}^{(0)} \rangle_{\mathrm{f}} \end{aligned} \tag{147}$$

Therefore we have

$$\langle \mathrm{Tr}(\xi_{\mathbf{y}}(\dot{\mathbf{u}}^{(1)}_{\mathrm{I}})) \rangle_{\mathrm{I}} + \langle \mathrm{Tr}(\xi_{\mathbf{y}}(\dot{\mathbf{u}}^{(1)}_{\mathrm{II}})) \rangle_{\mathrm{II}} = \nabla_{\mathbf{x}} \cdot \langle \mathbf{v}^{(0)} \rangle_{\mathrm{f}}. \tag{148}$$

Using Eqs. (127) and (128) with (140) we have that

$$\begin{aligned} \xi_{\mathbf{y}}(\dot{\mathbf{u}}^{(1)}_{\mathrm{I}}) + \xi_{\mathbf{y}}(\dot{\mathbf{u}}^{(1)}_{\mathrm{II}}) &= \mathbb{M}_{\mathrm{I}} : \xi_{\mathbf{x}}(\dot{\mathbf{u}}^{(0)}_{\mathrm{I}}) + \mathbb{M}_{\mathrm{II}} : \xi_{\mathbf{x}}(\dot{\mathbf{u}}^{(0)}_{\mathrm{II}}) \\ &\quad + (Q_{\mathrm{I}} + Q_{\mathrm{II}}) \dot{p}^{(0)} \end{aligned} \tag{149}$$

Then using (149), Eq. (148) becomes

$$\begin{aligned} \nabla_{\mathbf{x}} \cdot \langle \mathbf{v}^{(0)} \rangle_{\mathrm{f}} &= \langle \mathrm{Tr}(\mathbb{M}_{\mathrm{I}}) \rangle_{\mathrm{I}} : \xi_{\mathbf{x}}(\dot{\mathbf{u}}^{(0)}_{\mathrm{I}}) + \langle \mathrm{Tr}(\mathbb{M}_{\mathrm{II}}) \rangle_{\mathrm{II}} : \xi_{\mathbf{x}}(\dot{\mathbf{u}}^{(0)}_{\mathrm{II}}) \\ &\quad + \langle \mathrm{Tr}(Q_{\mathrm{I}} + Q_{\mathrm{II}}) \rangle_s \dot{p}^{(0)} \end{aligned} \tag{150}$$

We can then rewrite (150) using (106) as

$$\begin{aligned} &\nabla_{\mathbf{x}} \cdot (-\langle \mathsf{W} \rangle_{\mathrm{f}} \nabla_{\mathbf{x}} p^{(0)} + \langle \mathsf{G} \rangle_{\mathrm{f}} \dot{\mathbf{u}}^{(0)}_{\mathrm{I}} + \langle \mathsf{L} \rangle_{\mathrm{f}} \dot{\mathbf{u}}^{(0)}_{\mathrm{II}}) \\ &= \langle \mathrm{Tr}(\mathbb{M}_{\mathrm{I}}) \rangle_{\mathrm{I}} : \xi_{\mathbf{x}}(\dot{\mathbf{u}}^{(0)}_{\mathrm{I}}) + \langle \mathrm{Tr}(\mathbb{M}_{\mathrm{II}}) \rangle_{\mathrm{II}} : \xi_{\mathbf{x}}(\dot{\mathbf{u}}^{(0)}_{\mathrm{II}}) \\ &+ \mathrm{Tr}(\langle Q_{\mathrm{I}} \rangle_{\mathrm{I}} + \langle Q_{\mathrm{II}} \rangle_{\mathrm{II}}) \dot{p}^{(0)} \end{aligned} \tag{151}$$

By expanding the left hand side of (151) we can then rearrange to obtain the following expression for $\dot{p}^{(0)}$. That is

$$\begin{aligned} \dot{p}^{(0)} = \frac{1}{\mathrm{Tr}(\langle Q_{\mathrm{I}} \rangle_{\mathrm{I}} + \langle Q_{\mathrm{II}} \rangle_{\mathrm{II}})} \Big(&- \nabla_{\mathbf{x}} \cdot (\langle \mathsf{W} \rangle_{\mathrm{f}} \nabla_{\mathbf{x}} p^{(0)}) \\ &+ (\nabla_{\mathbf{x}} \cdot \langle \mathsf{G} \rangle^{\mathrm{T}}_{\mathrm{f}}) \cdot \dot{\mathbf{u}}^{(0)}_{\mathrm{I}} + (\nabla_{\mathbf{x}} \cdot \langle \mathsf{L} \rangle^{\mathrm{T}}_{\mathrm{f}}) \cdot \dot{\mathbf{u}}^{(0)}_{\mathrm{II}} \\ &+ (\langle \mathsf{G} \rangle_{\mathrm{f}} - \langle \mathrm{Tr}(\mathbb{M}_{\mathrm{I}}) \rangle_{\mathrm{I}}) : \xi_{\mathbf{x}}(\dot{\mathbf{u}}^{(0)}_{\mathrm{I}}) + (\langle \mathsf{L} \rangle_{\mathrm{f}} \\ &- \langle \mathrm{Tr}(\mathbb{M}_{\mathrm{II}}) \rangle_{\mathrm{II}}) : \xi_{\mathbf{x}}(\dot{\mathbf{u}}^{(0)}_{\mathrm{II}}) \Big) \end{aligned} \tag{152}$$

We can then define

$$M = \frac{-1}{\mathrm{Tr}(\langle Q_{\mathrm{I}} \rangle_{\mathrm{I}} + \langle Q_{\mathrm{II}} \rangle_{\mathrm{II}})} \quad \text{and} \quad \boldsymbol{\alpha}_{\mathrm{I}} = \langle \mathsf{G} \rangle_{\mathrm{f}} - \langle \mathrm{Tr}(\mathbb{M}_{\mathrm{I}}) \rangle_{\mathrm{I}}$$
$$\text{and} \quad \boldsymbol{\alpha}_{\mathrm{II}} = \langle \mathsf{L} \rangle_{\mathrm{f}} - \langle \mathrm{Tr}(\mathbb{M}_{\mathrm{II}}) \rangle_{\mathrm{II}} \tag{153}$$

where M is the Biot's modulus for the system and $\boldsymbol{\alpha}_{\mathrm{I}}$ and $\boldsymbol{\alpha}_{\mathrm{II}}$ remind of the Biot's tensor of coefficients, but here we have one for each elastic phase. Using this notation we can rewrite (152) as

$$\begin{aligned} \dot{p}^{(0)} = -M \Big(&- \nabla_{\mathbf{x}} \cdot (\langle \mathsf{W} \rangle_{\mathrm{f}} \nabla_{\mathbf{x}} p^{(0)}) + (\nabla_{\mathbf{x}} \cdot \langle \mathsf{G} \rangle^{\mathrm{T}}_{\mathrm{f}}) \cdot \dot{\mathbf{u}}^{(0)}_{\mathrm{I}} \\ &+ (\nabla_{\mathbf{x}} \cdot \langle \mathsf{L} \rangle^{\mathrm{T}}_{\mathrm{f}}) \cdot \dot{\mathbf{u}}^{(0)}_{\mathrm{II}} + \boldsymbol{\alpha}_{\mathrm{I}} : \xi_{\mathbf{x}}(\dot{\mathbf{u}}^{(0)}_{\mathrm{I}}) \\ &+ \boldsymbol{\alpha}_{\mathrm{II}} : \xi_{\mathbf{x}}(\dot{\mathbf{u}}^{(0)}_{\mathrm{II}}) \Big). \end{aligned} \tag{154}$$

Then we can finally divide through by M to obtain

$$\begin{aligned} \frac{\dot{p}^{(0)}}{M} &= \nabla_{\mathbf{x}} \cdot (\langle \mathsf{W} \rangle_{\mathrm{f}} \nabla_{\mathbf{x}} p^{(0)}) - (\nabla_{\mathbf{x}} \cdot \langle \mathsf{G} \rangle^{\mathrm{T}}_{\mathrm{f}}) \cdot \dot{\mathbf{u}}^{(0)}_{\mathrm{I}} \\ &\quad - (\nabla_{\mathbf{x}} \cdot \langle \mathsf{L} \rangle^{\mathrm{T}}_{\mathrm{f}}) \cdot \dot{\mathbf{u}}^{(0)}_{\mathrm{II}} - \boldsymbol{\alpha}_{\mathrm{I}} : \xi_{\mathbf{x}}(\dot{\mathbf{u}}^{(0)}_{\mathrm{I}}) \\ &\quad - \boldsymbol{\alpha}_{\mathrm{II}} : \xi_{\mathbf{x}}(\dot{\mathbf{u}}^{(0)}_{\mathrm{II}}). \end{aligned} \tag{155}$$

We have now derived all the equations required to be able to state our macroscale model for two non-interacting solid phases percolated by a viscous fluid.

4. The macroscale model

The macroscale model for our material describes the effective poroelastic behaviour in terms of the pore pressure, the average fluid velocity and the elastic displacement of the individual elastic phases. We now state the governing equations which are

$$\langle \mathbf{v}^{(0)} \rangle_{\mathrm{f}} = -\langle \mathsf{W} \rangle_{\mathrm{f}} \nabla_{\mathbf{x}} p^{(0)} + \langle \mathsf{G} \rangle_{\mathrm{f}} \dot{\mathbf{u}}^{(0)}_{\mathrm{I}} + \langle \mathsf{L} \rangle_{\mathrm{f}} \dot{\mathbf{u}}^{(0)}_{\mathrm{II}}, \tag{156}$$

$$\begin{aligned} &\nabla_{\mathbf{x}} \cdot \langle \boldsymbol{\sigma}^{(0)}_{\mathrm{I}} \rangle_{\mathrm{I}} + \left(\int_{\Gamma_{\mathrm{I}}} \mathbf{n}_{\mathrm{I}} \otimes \mathbf{P} \, \mathrm{dS} - \int_{\Gamma_{\mathrm{I}}} \xi_{\mathbf{y}}(\mathsf{W}) \mathbf{n}_{\mathrm{I}} \, \mathrm{dS} \right) \nabla_{\mathbf{x}} p^{(0)} \\ &+ \left(\int_{\Gamma_{\mathrm{I}}} \xi_{\mathbf{y}}(\mathsf{G}) \mathbf{n}_{\mathrm{I}} \, \mathrm{dS} - \int_{\Gamma_{\mathrm{I}}} \mathbf{n}_{\mathrm{I}} \otimes \mathbf{H} \, \mathrm{dS} \right) \dot{\mathbf{u}}^{(0)}_{\mathrm{I}} \\ &+ \left(\int_{\Gamma_{\mathrm{I}}} \xi_{\mathbf{y}}(\mathsf{L}) \mathbf{n}_{\mathrm{I}} \, \mathrm{dS} - \int_{\Gamma_{\mathrm{I}}} \mathbf{n}_{\mathrm{I}} \otimes \mathbf{S} \, \mathrm{dS} \right) \dot{\mathbf{u}}^{(0)}_{\mathrm{II}} = 0, \end{aligned} \tag{157}$$

$$\langle \boldsymbol{\sigma}^{(0)}_{\mathrm{I}} \rangle_{\mathrm{I}} = \langle \mathbb{C}_{\mathrm{I}}\mathbb{M}_{\mathrm{I}} + \mathbb{C}_{\mathrm{I}} \rangle_{\mathrm{I}} \xi_{\mathbf{x}}(\mathbf{u}^{(0)}_{\mathrm{I}}) + \langle \mathbb{C}_{\mathrm{I}} Q_{\mathrm{I}} \rangle_{\mathrm{I}} p^{(0)}, \tag{158}$$

$$\begin{aligned} &\nabla_{\mathbf{x}} \cdot \langle \boldsymbol{\sigma}^{(0)}_{\mathrm{II}} \rangle_{\mathrm{II}} + \left(\int_{\Gamma_{\mathrm{II}}} \mathbf{n}_{\mathrm{II}} \otimes \mathbf{P} \, \mathrm{dS} - \int_{\Gamma_{\mathrm{II}}} \xi_{\mathbf{y}}(\mathsf{W}) \mathbf{n}_{\mathrm{II}} \, \mathrm{dS} \right) \nabla_{\mathbf{x}} p^{(0)} \\ &+ \left(\int_{\Gamma_{\mathrm{II}}} \xi_{\mathbf{y}}(\mathsf{G}) \mathbf{n}_{\mathrm{II}} \, \mathrm{dS} - \int_{\Gamma_{\mathrm{II}}} \mathbf{n}_{\mathrm{II}} \otimes \mathbf{H} \, \mathrm{dS} \right) \dot{\mathbf{u}}^{(0)}_{\mathrm{I}} \\ &+ \left(\int_{\Gamma_{\mathrm{II}}} \xi_{\mathbf{y}}(\mathsf{L}) \mathbf{n}_{\mathrm{II}} \, \mathrm{dS} - \int_{\Gamma_{\mathrm{II}}} \mathbf{n}_{\mathrm{II}} \otimes \mathbf{S} \, \mathrm{dS} \right) \dot{\mathbf{u}}^{(0)}_{\mathrm{II}} = 0, \end{aligned} \tag{159}$$

$$\langle \boldsymbol{\sigma}^{(0)}_{\mathrm{II}} \rangle_{\mathrm{II}} = \langle \mathbb{C}_{\mathrm{II}}\mathbb{M}_{\mathrm{II}} + \mathbb{C}_{\mathrm{II}} \rangle_{\mathrm{II}} \xi_{\mathbf{x}}(\mathbf{u}^{(0)}_{\mathrm{II}}) + \langle \mathbb{C}_{\mathrm{II}} Q_{\mathrm{II}} \rangle_{\mathrm{II}} p^{(0)}, \tag{160}$$

$$\begin{aligned} \dot{p}^{(0)} = \frac{1}{\mathrm{Tr}(\langle Q_{\mathrm{I}} \rangle_{\mathrm{I}} + \langle Q_{\mathrm{II}} \rangle_{\mathrm{II}})} \Big(&- \nabla_{\mathbf{x}} \cdot (\langle \mathsf{W} \rangle_{\mathrm{f}} \nabla_{\mathbf{x}} p^{(0)}) \\ &+ (\nabla_{\mathbf{x}} \cdot \langle \mathsf{G} \rangle^{\mathrm{T}}_{\mathrm{f}}) \cdot \dot{\mathbf{u}}^{(0)}_{\mathrm{I}} + (\nabla_{\mathbf{x}} \cdot \langle \mathsf{L} \rangle^{\mathrm{T}}_{\mathrm{f}}) \cdot \dot{\mathbf{u}}^{(0)}_{\mathrm{II}} + (\langle \mathsf{G} \rangle_{\mathrm{f}} \\ &- \langle \mathrm{Tr}(\mathbb{M}_{\mathrm{I}}) \rangle_{\mathrm{I}}) : \xi_{\mathbf{x}}(\dot{\mathbf{u}}^{(0)}_{\mathrm{I}}) + (\langle \mathsf{L} \rangle_{\mathrm{f}} - \langle \mathrm{Tr}(\mathbb{M}_{\mathrm{II}}) \rangle_{\mathrm{II}}) : \xi_{\mathbf{x}}(\dot{\mathbf{u}}^{(0)}_{\mathrm{II}}) \Big) \end{aligned} \tag{161}$$

where we have that $p^{(0)}$ is the macroscale pressure, $\mathbf{u}^{(0)}_{\mathrm{I}}$ is the solid displacement in the fibre network, $\mathbf{u}^{(0)}_{\mathrm{II}}$ is the solid displacement in the matrix, $\dot{\mathbf{u}}^{(0)}_{\mathrm{I}}$ is the solid velocity in the fibres and $\dot{\mathbf{u}}^{(0)}_{\mathrm{II}}$ is the solid velocity in the matrix. The novel model comprises the equation governing the fluid flow (156). This equation is a modified Darcy flow that accounts for the influence of the fibre network and the matrix on the fluid contained between them. That is, it depends on the geometry and elastic properties of the two solid phases. We have that (157) is the balance equation for our fibre network portion of the material with leading order stress given by (158). We have that (159) is the balance equation for our matrix portion of the material with the leading order stress given by (160). The leading order stresses for each of the phases are of poroelastic type. Due to the discontinuity in the leading order elastic displacements we can define two effective elasticity tensors (one in each elastic phase). These are given by

$$\widetilde{\mathbb{C}}_{\mathrm{I}} = \langle \mathbb{C}_{\mathrm{I}}\mathbb{M}_{\mathrm{I}} + \mathbb{C}_{\mathrm{I}} \rangle_{\mathrm{I}} \quad \text{and} \quad \widetilde{\mathbb{C}}_{\mathrm{II}} = \langle \mathbb{C}_{\mathrm{II}}\mathbb{M}_{\mathrm{II}} + \mathbb{C}_{\mathrm{II}} \rangle_{\mathrm{II}}. \tag{162}$$

The final equation of the novel macroscale model is the conservation of mass equation. The second and third terms on the RHS (the divergence of the second rank tensors G and L) describe the volume changes related to the deformation and influence of the two elastic phases that are not in contact and can be viewed as a correction term that maintains the conservation of mass in the system.

The first Eq. (156) is the modified Darcy's flow that is written in terms of the absolute velocity $\mathbf{v}^{(0)}$. This equation takes into consideration the effects of the pressure as well as the influence of the solid velocities of both the solid phases. The tensors of coefficients W, G and L are to be obtained by solving the newly arising fluid cell problems (103), (104), (105) which then encode the influence that these two solid structures have on the fluid that flows in the void.

The key novelty of this work resides in considering the influence of two different discontinuous elastic phases on the fluid that is contained between them. This is reflected in the newly arising fluid cell problems (103), (104), (105). Solving these cell problem encodes the details of the geometry and stiffness of the microstructure in the tensors which appear in the fluid flow equation and the conservation of mass equation in the macroscale model. So that is, we are accounting for the microscale complexity within the novel macroscale model. We also have the addition of two new balance equations that are required to close the problem since we do not have the continuity of elastic phases. These new balance equations consider each phase and contain surface integrals of terms arising from the fluid cell problems. This means that we are taking into consideration each elastic phase and the influence of the fluid on it separately. The novel model here cannot strictly be considered of standard *poroelastic-type* in the sense of the definition provided in Miller and Penta (2020).

Remark 6 (*Limit Cases*)**.** In the case that the fibres are not fully embedded in the fluid but is in fact in contact with the matrix we can recover (Miller and Penta, 2020). To obtain this model we assume that we have the continuity of the elastic displacements $\mathbf{u}_{\mathrm{I}}^{(0)}$, $\mathbf{u}_{\mathrm{II}}^{(0)}$ and the solid velocities $\dot{\mathbf{u}}_{\mathrm{I}}^{(0)}$, $\dot{\mathbf{u}}_{\mathrm{II}}^{(0)}$. We will begin with considering (156) assuming the continuity of leading order solid velocities

$$\langle \mathbf{v}^{(0)} \rangle_{\mathrm{f}} = -\langle \mathsf{W} \rangle_{\mathrm{f}} \nabla_{\mathbf{x}} p^{(0)} - (\langle \mathsf{G} + \mathsf{L} \rangle_{\mathrm{f}}) \dot{\mathbf{u}}^{(0)} \tag{163}$$

We have that $\langle \mathsf{G}+\mathsf{L} \rangle_{\mathrm{f}}$ is the average of the identity over the fluid domain which we can write as $\langle \mathsf{I} \rangle_{\mathrm{f}}$ and this is equivalent to $\phi \mathsf{I}$. To see that G+L is the identity we can consider the summation of the cell problems (104) and (105). This means we can rewrite (163)

$$\langle \mathbf{v}^{(0)} \rangle_{\mathrm{f}} = -\langle \mathsf{W} \rangle_{\mathrm{f}} \nabla_{\mathbf{x}} p^{(0)} - \phi \dot{\mathbf{u}}^{(0)} \tag{164}$$

Then by using the definition of the relative fluid–solid velocity defined in Miller and Penta (2020) as

$$\langle \mathbf{w}^{(0)} \rangle_{\mathrm{f}} = \langle \mathbf{v}^{(0)} \rangle_{\mathrm{f}} - \phi \dot{\mathbf{u}}^{(0)} \tag{165}$$

we can write (164) as

$$\langle \mathbf{w}^{(0)} \rangle_{\mathrm{f}} = -\langle \mathsf{W} \rangle_{\mathrm{f}} \nabla_{\mathbf{x}} p^{(0)}, \tag{166}$$

which is exactly Darcy's law as found in Miller and Penta (2020) for poroelastic composites.

In this work we propose two separate balance laws, one for the fibre network portion of the material (157) and one for the matrix portion (159). This is since the two elastic phases are fully decoupled because of the fluid that is between them. We can however recover the balance equation of Miller and Penta (2020) by summing up (157) and (159) and assuming the continuity of the two elastic phases. That is

$$\begin{aligned}
&\nabla_{\mathbf{x}} \cdot \langle \boldsymbol{\sigma}_{\mathrm{I}}^{(0)} \rangle_{\mathrm{I}} + \left(\int_{\Gamma_{\mathrm{I}}} \mathbf{n}_{\mathrm{I}} \otimes \mathbf{P} \, \mathrm{dS} - \int_{\Gamma_{\mathrm{I}}} \xi_{\mathbf{y}}(\mathsf{W}) \mathbf{n}_{\mathrm{I}} \, \mathrm{dS} \right) \nabla_{\mathbf{x}} p^{(0)} \\
&+ \left(\int_{\Gamma_{\mathrm{I}}} \xi_{\mathbf{y}}(\mathsf{G}) \mathbf{n}_{\mathrm{I}} \, \mathrm{dS} - \int_{\Gamma_{\mathrm{I}}} \mathbf{n}_{\mathrm{I}} \otimes \mathbf{H} \, \mathrm{dS} \right) \dot{\mathbf{u}}_{\mathrm{I}}^{(0)} \\
&+ \left(\int_{\Gamma_{\mathrm{I}}} \xi_{\mathbf{y}}(\mathsf{L}) \mathbf{n}_{\mathrm{I}} \, \mathrm{dS} - \int_{\Gamma_{\mathrm{I}}} \mathbf{n}_{\mathrm{I}} \otimes \mathbf{S} \, \mathrm{dS} \right) \dot{\mathbf{u}}_{\mathrm{II}}^{(0)} \\
&+ \nabla_{\mathbf{x}} \cdot \langle \boldsymbol{\sigma}_{\mathrm{II}}^{(0)} \rangle_{\mathrm{II}} + \left(\int_{\Gamma_{\mathrm{II}}} \mathbf{n}_{\mathrm{II}} \otimes \mathbf{P} \, \mathrm{dS} - \int_{\Gamma_{\mathrm{II}}} \xi_{\mathbf{y}}(\mathsf{W}) \mathbf{n}_{\mathrm{II}} \, \mathrm{dS} \right) \nabla_{\mathbf{x}} p^{(0)} \\
&+ \left(\int_{\Gamma_{\mathrm{II}}} \xi_{\mathbf{y}}(\mathsf{G}) \mathbf{n}_{\mathrm{II}} \, \mathrm{dS} - \int_{\Gamma_{\mathrm{II}}} \mathbf{n}_{\mathrm{II}} \otimes \mathbf{H} \, \mathrm{dS} \right) \dot{\mathbf{u}}_{\mathrm{I}}^{(0)} \\
&+ \left(\int_{\Gamma_{\mathrm{II}}} \xi_{\mathbf{y}}(\mathsf{L}) \mathbf{n}_{\mathrm{II}} \, \mathrm{dS} - \int_{\Gamma_{\mathrm{II}}} \mathbf{n}_{\mathrm{II}} \otimes \mathbf{S} \, \mathrm{dS} \right) \dot{\mathbf{u}}_{\mathrm{II}}^{(0)} = 0,
\end{aligned} \tag{167}$$

We can combine the terms as follows and assume that $\dot{\mathbf{u}}_{\mathrm{I}}^{(0)} = \dot{\mathbf{u}}_{\mathrm{II}}^{(0)} = \dot{\mathbf{u}}^{(0)}$ to obtain

$$\begin{aligned}
&\nabla_{\mathbf{x}} \cdot \langle \boldsymbol{\sigma}_{\mathrm{I}}^{(0)} \rangle_{\mathrm{I}} + \left(\int_{\Gamma_{\mathrm{I}}} \mathbf{n}_{\mathrm{I}} \otimes \mathbf{P} \, \mathrm{dS} - \int_{\Gamma_{\mathrm{I}}} \xi_{\mathbf{y}}(\mathsf{W}) \mathbf{n}_{\mathrm{I}} \, \mathrm{dS} \right. \\
&\left. + \int_{\Gamma_{\mathrm{II}}} \mathbf{n}_{\mathrm{II}} \otimes \mathbf{P} \, \mathrm{dS} - \int_{\Gamma_{\mathrm{II}}} \xi_{\mathbf{y}}(\mathsf{W}) \mathbf{n}_{\mathrm{II}} \, \mathrm{dS} \right) \nabla_{\mathbf{x}} p^{(0)} \\
&+ \left(\int_{\Gamma_{\mathrm{I}}} \xi_{\mathbf{y}}(\mathsf{G}) \mathbf{n}_{\mathrm{I}} \, \mathrm{dS} - \int_{\Gamma_{\mathrm{I}}} \mathbf{n}_{\mathrm{I}} \otimes \mathbf{H} \, \mathrm{dS} + \int_{\Gamma_{\mathrm{I}}} \xi_{\mathbf{y}}(\mathsf{L}) \mathbf{n}_{\mathrm{I}} \, \mathrm{dS} \right. \\
&- \int_{\Gamma_{\mathrm{I}}} \mathbf{n}_{\mathrm{I}} \otimes \mathbf{S} \, \mathrm{dS} + \int_{\Gamma_{\mathrm{II}}} \xi_{\mathbf{y}}(\mathsf{G}) \mathbf{n}_{\mathrm{II}} \, \mathrm{dS} - \int_{\Gamma_{\mathrm{II}}} \mathbf{n}_{\mathrm{II}} \otimes \mathbf{H} \, \mathrm{dS} \\
&\left. + \int_{\Gamma_{\mathrm{II}}} \xi_{\mathbf{y}}(\mathsf{L}) \mathbf{n}_{\mathrm{II}} \, \mathrm{dS} - \int_{\Gamma_{\mathrm{II}}} \mathbf{n}_{\mathrm{II}} \otimes \mathbf{S} \, \mathrm{dS} \right) \dot{\mathbf{u}}^{(0)} \\
&+ \nabla_{\mathbf{x}} \cdot \langle \boldsymbol{\sigma}_{\mathrm{II}}^{(0)} \rangle_{\mathrm{II}} = 0,
\end{aligned} \tag{168}$$

Since we now have terms on both Γ_{I} and Γ_{II} we have the complete boundary of the fluid domain, so we are able to reverse the divergence theorem to get all the integrals in the fluid domain. We also use the definition of the symmetric part of the gradient operator (9). That is

$$\begin{aligned}
&\nabla_{\mathbf{x}} \cdot \langle \boldsymbol{\sigma}_{\mathrm{I}}^{(0)} \rangle_{\mathrm{I}} - \left(\int_{\Omega_{\mathrm{f}}} \nabla_{\mathbf{y}} \mathbf{P} \mathbf{d}\mathbf{y} - \int_{\Omega_{\mathrm{f}}} \nabla_{\mathbf{y}}^2 \mathsf{W}^{\mathrm{T}} \mathbf{d}\mathbf{y} \right. \\
&\left. - \int_{\Gamma_{\mathrm{I}}} \nabla_{\mathbf{y}} (\nabla_{\mathbf{y}} \cdot \mathsf{W}^{\mathrm{T}}) \mathbf{d}\mathbf{y} \right) \nabla_{\mathbf{x}} p^{(0)} - \left(\int_{\Omega_{\mathrm{f}}} \nabla_{\mathbf{y}}^2 \mathsf{G}^{\mathrm{T}} \mathbf{d}\mathbf{y} \right. \\
&+ \int_{\Omega_{\mathrm{I}}} \nabla_{\mathbf{y}} (\nabla_{\mathbf{y}} \cdot \mathsf{G}^{\mathrm{T}}) \mathbf{d}\mathbf{y} - \int_{\Omega_{\mathrm{f}}} \nabla_{\mathbf{y}} \mathbf{H} \mathbf{d}\mathbf{y} + \int_{\Omega_{\mathrm{f}}} \nabla_{\mathbf{y}}^2 \mathsf{L}^{\mathrm{T}} \mathbf{d}\mathbf{y} \\
&\left. + \int_{\Omega_{\mathrm{f}}} \nabla_{\mathbf{y}} (\nabla_{\mathbf{y}} \cdot \mathsf{L}^{\mathrm{T}}) \mathbf{d}\mathbf{y} - \int_{\Omega_{\mathrm{f}}} \nabla_{\mathbf{y}} \mathbf{S} \mathbf{d}\mathbf{y} \right) \dot{\mathbf{u}}^{(0)} \\
&+ \nabla_{\mathbf{x}} \cdot \langle \boldsymbol{\sigma}_{\mathrm{II}}^{(0)} \rangle_{\mathrm{II}} = 0.
\end{aligned} \tag{169}$$

Then we can use the cell problems (104) and (105) to cancel all the integrals multiplying the $\dot{\mathbf{u}}^{(0)}$. That is

$$\begin{aligned}
&\nabla_{\mathbf{x}} \cdot \langle \boldsymbol{\sigma}_{\mathrm{I}}^{(0)} \rangle_{\mathrm{I}} - \left(\int_{\Omega_{\mathrm{f}}} \nabla_{\mathbf{y}} \mathbf{P} \mathbf{d}\mathbf{y} - \int_{\Omega_{\mathrm{f}}} \nabla_{\mathbf{y}}^2 \mathsf{W}^{\mathrm{T}} \mathbf{d}\mathbf{y} \right. \\
&\left. - \int_{\Gamma_{\mathrm{I}}} \nabla_{\mathbf{y}} (\nabla_{\mathbf{y}} \cdot \mathsf{W}^{\mathrm{T}}) \mathbf{d}\mathbf{y} \right) \nabla_{\mathbf{x}} p^{(0)} \\
&+ \nabla_{\mathbf{x}} \cdot \langle \boldsymbol{\sigma}_{\mathrm{II}}^{(0)} \rangle_{\mathrm{II}} = 0.
\end{aligned} \tag{170}$$

Then using cell problem (103) we can replace the first two integrals using the first equation and the third integral is zero due to the second equation. That is

$$\begin{aligned}
&\nabla_{\mathbf{x}} \cdot \langle \boldsymbol{\sigma}_{\mathrm{I}}^{(0)} \rangle_{\mathrm{I}} - \left(\int_{\Omega_{\mathrm{f}}} \mathrm{I} \mathbf{d}\mathbf{y} \right) \nabla_{\mathbf{x}} p^{(0)} \\
&+ \nabla_{\mathbf{x}} \cdot \langle \boldsymbol{\sigma}_{\mathrm{II}}^{(0)} \rangle_{\mathrm{II}} = 0.
\end{aligned} \tag{171}$$

The integral of the identity over the fluid domain become the fluid volume fraction ϕ, so the final balance equation can be written as

$$\nabla_{\mathbf{x}} \cdot \langle \boldsymbol{\sigma}_{\mathrm{I}}^{(0)} \rangle_{\mathrm{I}} + \nabla_{\mathbf{x}} \cdot \langle \boldsymbol{\sigma}_{\mathrm{II}}^{(0)} \rangle_{\mathrm{II}} - \phi \nabla_{\mathbf{x}} p^{(0)} = 0, \tag{172}$$

or equivalently

$$\nabla_{\mathbf{x}} \cdot (\langle \boldsymbol{\sigma}_{\mathrm{I}}^{(0)} \rangle_{\mathrm{I}} + \langle \boldsymbol{\sigma}_{\mathrm{II}}^{(0)} \rangle_{\mathrm{I}} - \phi p^{(0)} \mathrm{I}) = 0. \tag{173}$$

The terms $\langle \boldsymbol{\sigma}_{\mathrm{I}}^{(0)} \rangle_{\mathrm{I}} + \langle \boldsymbol{\sigma}_{\mathrm{II}}^{(0)} \rangle_{\mathrm{I}} - \phi p^{(0)} \mathrm{I}$ are called $\mathsf{T}_{\mathrm{Eff}}$ in Miller and Penta (2020) and are the constitutive law. Using (158) and (160) and assuming the continuity we can write, using the notation $\langle \boldsymbol{\sigma}_{\mathrm{I}}^{(0)} \rangle_{\mathrm{I}} + \langle \boldsymbol{\sigma}_{\mathrm{II}}^{(0)} \rangle_{\mathrm{I}} - \phi p^{(0)} \mathrm{I} = \mathsf{T}_{\mathrm{Eff}}$,

$$\mathsf{T}_{\mathrm{Eff}} = (\langle \mathbb{C}_{\mathrm{I}} \mathbb{M}_{\mathrm{I}} + \mathbb{C}_{\mathrm{I}} \rangle_{\mathrm{I}} + \langle \mathbb{C}_{\mathrm{II}} \mathbb{M}_{\mathrm{II}} + \mathbb{C}_{\mathrm{II}} \rangle_{\mathrm{II}}) : \xi_{\mathbf{x}}(\mathbf{u}^{(0)})$$

$$+ (\langle \mathbb{C}_{\mathrm{I}} Q_{\mathrm{I}} \rangle_{\mathrm{I}} + \langle \mathbb{C}_{\mathrm{II}} Q_{\mathrm{II}} \rangle_{\mathrm{II}} - \phi \mathrm{I}) p^{(0)}, \tag{174}$$

which is exactly the constitutive law found in Miller and Penta (2020).

We must also enforce the limit in the conservation of mass Eq. (161). Assuming the continuity of solid velocities we can rewrite as

$$\begin{aligned} \dot{p}^{(0)} = \frac{1}{\mathrm{Tr}(\langle Q_{\mathrm{I}} \rangle_{\mathrm{I}} + \langle Q_{\mathrm{II}} \rangle_{\mathrm{II}})} \Big(& -\nabla_{\mathbf{x}} \cdot (\langle \mathsf{W} \rangle_{\mathrm{f}} \nabla_{\mathbf{x}} p^{(0)}) \\ & + (\nabla_{\mathbf{x}} \cdot \langle \mathsf{G} \rangle_{\mathrm{f}}^{\mathrm{T}} + \nabla_{\mathbf{x}} \cdot \langle \mathsf{L} \rangle_{\mathrm{f}}^{\mathrm{T}}) \cdot \dot{\mathbf{u}}^{(0)} + (\langle \mathsf{G} \rangle_{\mathrm{f}} + \langle \mathsf{L} \rangle_{\mathrm{f}} \\ & - \langle \mathrm{Tr}(\mathbb{M}_{\mathrm{I}}) \rangle_{\mathrm{I}} - \langle \mathrm{Tr}(\mathbb{M}_{\mathrm{II}}) \rangle_{\mathrm{II}}) : \xi_{\mathbf{x}}(\dot{\mathbf{u}}^{(0)}) \Big) \end{aligned} \tag{175}$$

We can use the fact that $\langle \mathsf{G} + \mathsf{L} \rangle_{\mathrm{f}}$ is the average of the identity over the fluid domain to rewrite (175) as

$$\begin{aligned} \dot{p}^{(0)} = \frac{1}{\mathrm{Tr}(\langle Q_{\mathrm{I}} \rangle_{\mathrm{I}} + \langle Q_{\mathrm{II}} \rangle_{\mathrm{II}})} \Big(& -\nabla_{\mathbf{x}} \cdot (\langle \mathsf{W} \rangle_{\mathrm{f}} \nabla_{\mathbf{x}} p^{(0)}) \\ & + (\nabla_{\mathbf{x}} \cdot \langle I \rangle_{\mathrm{f}}) \cdot \dot{\mathbf{u}}^{(0)} + (\langle I \rangle_{\mathrm{f}} - \langle \mathrm{Tr}(\mathbb{M}_{\mathrm{I}}) \rangle_{\mathrm{I}} \\ & - \langle \mathrm{Tr}(\mathbb{M}_{\mathrm{II}}) \rangle_{\mathrm{II}}) : \xi_{\mathbf{x}}(\dot{\mathbf{u}}^{(0)}) \Big) \end{aligned} \tag{176}$$

Since the divergence of the identity is zero the second term disappears and we can finally write as

$$\begin{aligned} \dot{p}^{(0)} = \frac{1}{\mathrm{Tr}(\langle Q_{\mathrm{I}} \rangle_{\mathrm{I}} + \langle Q_{\mathrm{II}} \rangle_{\mathrm{II}})} \Big(& -\nabla_{\mathbf{x}} \cdot (\langle \mathsf{W} \rangle_{\mathrm{f}} \nabla_{\mathbf{x}} p^{(0)}) + (\phi I \\ & - \langle \mathrm{Tr}(\mathbb{M}_{\mathrm{I}}) \rangle_{\mathrm{I}} - \langle \mathrm{Tr}(\mathbb{M}_{\mathrm{II}}) \rangle_{\mathrm{II}}) : \xi_{\mathbf{x}}(\dot{\mathbf{u}}^{(0)}) \Big) \end{aligned} \tag{177}$$

This is the conservation of mass equation found in Miller and Penta (2020).

5. Applicability of the model and numerical results

In this section we discuss important examples of real world problems where our novel model can be applied Section 5.1. We also provide an overview of the numerical simulations and results we have obtained for our model Section 5.2.

5.1. Potential applications

We first note that this model cannot be deduced as a special case of Miller and Penta (2020). This is due to the fact that the discontinuity of the elastic phases changes the nature of the differential cell problems and consequently the model coefficients are different. That is, this model is able to account for the behaviour of two different elastic phases and the influence they have on the fluid flowing between them.

By considering this geometry we are able to account for some very interesting applications in biology, medical devices and porous scaffolds. Within modelling of the perfusion of biological tissues such as the heart or brain or indeed the modelling of hard hierarchical tissues such as the bones this model could be useful.

The human heart has four chambers each of which has a muscular wall with three distinct layers, the endocardium, the myocardium, and the epicardium. The endocardium and epicardium are the thin inner and outer layers, whereas the myocardium is the middle contractile layer. It is supplied by the coronary arteries and is the layer most affected by a variety of diseases, e.g., myocardial infarction, angina and the effects of ageing. For this reason the modelling approach can be focussed on the myocardium (Whitaker, 2014; Weinhaus and Roberts, 2005; Purslow, 2008)

The myocardium has an embedded vasculature i.e., the blood vessels. When the vasculature supplying the heart becomes diseased via for example a build up of atherosclerosis or a blood clot then we potentially have a scenario like the geometry we have described here. The blood vessel embedded within the myocardium can be thought to be the pore of the matrix with the blood flowing through and the additional elastic phase can be a medical device used to treat disease or damage in the vessel (Kolodgie et al., 2007; Tsivgoulis et al., 2016). When the device is inserted it is small enough that it allows the blood to flow around but it then increases in size in order to capture the clot or disease building up in the artery. We can describe this scenario using our model since we can enlarge the embedded elastic inclusion/fibre to represent the medical device in a closed or open state depending on the point in treatment. Indeed, in Miller and Penta (2023a) a first approach has been made to investigate how physiologically observed microstructural changes induced by myocardial infarction impact the elastic parameters of the heart.

We should note that the current model uses linear elasticity and of course biological tissues such as the heart are indeed nonlinear. However, we could in fact obtain the approximate nonlinear behaviour by using a piecewise linear approach such as the one in Hu et al. (2003a,b). This method has the benefit of being able to approximate the behaviour whilst using simple, computationally cheap simulations.

This model is also applicable to hard hierarchical tissues, such as the bones. The bones have previously been considered as a poroelastic material in Cowin (1999), Perrin et al. (2019) and Cowin et al. (2009). The pores of the bones are filled with bone marrow, blood, or interstitial fluid and cells (Perrin et al., 2019; Cowin and Cardoso, 2015). In the context of bone remodelling, the process is regulated by mechanosensitive bone cells called osteocytes. These osteocytes are immersed in the interstitial fluid and can be found in the microscale pores (Perrin et al., 2019; Sánchez et al., 2021). This means that our model with the two elastic phases one of which is immersed in the fluid would be a good fit for examining the behaviour of bones.

Another potential application of this model is to living cells. Animal cells can be described by a poroelastic model due to their microstructure. The structure comprises elastic solid components such as the cytoskeleton, a variety of organelles and macromolecules, all of which are surrounded by the interstitial fluid (Moeendarbary et al., 2013). This is therefore another example of various different elastic phases that are not in contact yet are surrounded by fluid.

5.2. Numerical simulations

Within this subsection we first provide an overview of how the cell problems that we have derived in this work can be interpreted and solved numerically. We also indicate the portion of the domain on which each problem is to be solved. Then in Section 5.2.2 we investigate the Biot's Modulus for our model by first proving that it is positive and then backing up this theorem with numerical results. In Section 5.2.3 we then investigate the model coefficients that remind us formally of the Biot's tensor of coefficients.

5.2.1. Overview of the problems

The simulations for a linear poroelastic composite with continuity between the two elastic phases have recently been carried out in Miller and Penta (2023b). These simulations have then been used to investigate the effects of microstructural changes induced by myocardial infarction on the stiffness of the heart in Miller and Penta (2023a). By using a similar procedure to the one outlined in these works and Dehghani et al. (2018) we could solve the problems presented in this work using Comsol Multiphysics.

The cell problems (103), (104), (105) are to be solved on the fluid portion of our domain. Each of the fluid cell problems is a vector problem. The problem (103) is the typical Stokes problem for an incompressible fluid. Problems (104) and (104) take into consideration the fluid contact with either the matrix or the fibre network. By solving the fluid problems (103), (104), (105) this allows us to obtain the hydraulic conductivity tensor for our material. In Fig. 4 we show the fluid domain. It comprises 3 larger interconnected cylinders arranged orthogonally with 3 smaller interconnected cylinders removed from the centre.

Our two elastic phases are completely decoupled so we have a separate poroelastic problem for each of the phases. The cell problems

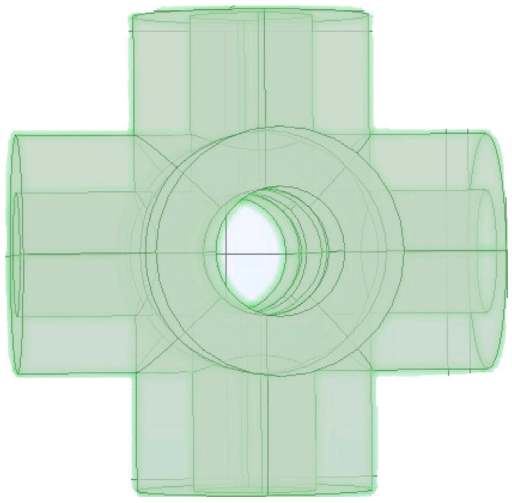

Fig. 4. Portion of the domain on which fluid cell problems have to be solved.

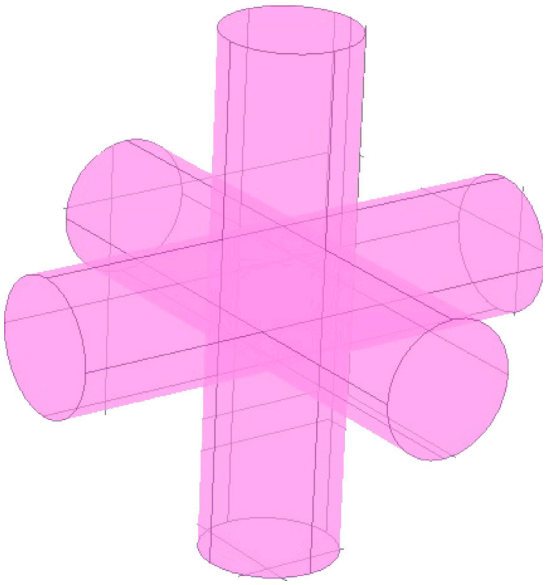

Fig. 5. Portion of the domain on which the elastic problem for the fibre network is to be solved.

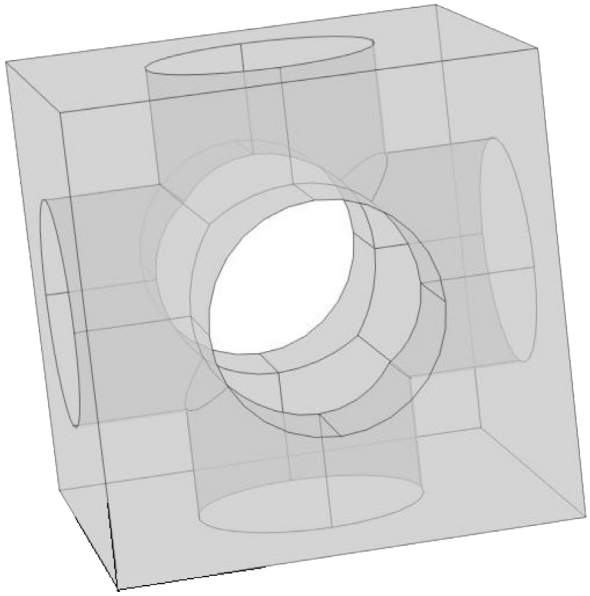

Fig. 6. Portion of the domain on which the elastic problem for the matrix is to be solved.

(129)–(130) and (133)–(134) are to be solved on the fibre network portion of the cell shown in Fig. 5 This is the three orthogonally arranged interconnected cylinders that are removed and leave the void within the fluid domain shown in Fig. 4. The second set of poroelastic cell problems (131)–(132) and (135)–(136) are for the matrix and are to be solved on the matrix portion of the cell shown in Fig. 6. This is the portion of the domain that remains after the removal of both the fluid and the elastic fibres. This geometry for the matrix portion alone is the typical periodic cell on which the elastic problems for standard Biot's poroelasticity are to be solved, see Dehghani et al. (2018). In order to solve problems (129)–(130) and (131)–(132) to find, $\xi_{\mathbf{y}}(A_{\mathrm{I}})$, $\xi_{\mathbf{y}}(A_{\mathrm{II}})$ (or equivalently $\mathbb{M}_{\mathrm{I}}$ and $\mathbb{M}_{\mathrm{II}}$) we are solving six elastic-type cell problems in which we consider $\xi_{\mathbf{y}}(A_{\mathrm{I}})$, $\xi_{\mathbf{y}}(A_{\mathrm{II}})$ as strains. We have the driving force behind the problems on the interface between the solid matrix and void or the fibre network and void depending on whether we are solving (129)–(130) for the fibres or (131)–(132) for the matrix. These forces account for the difference between the solid and the void where the fluid has been removed. The normal to the interface encodes the geometry of the voids. This allows for the computation of the drained coefficients $\mathbb{M}_{\mathrm{I}}$ and $\mathbb{M}_{\mathrm{II}}$.

We also solve the vector problems (133)–(134) and (135)–(136) to obtain $\xi_{\mathbf{y}}(\mathbf{a}_{\mathrm{I}})$, $\xi_{\mathbf{y}}(\mathbf{a}_{\mathrm{II}})$ (or equivalently Q_{I} and Q_{II}). We have that the driving forces for these problems are the normals to the interface between either the matrix and the void or the fibres and the void depending on which problem you are solving. The normal encodes the geometry of the voids and is used to compute the solution.

5.2.2. Properties and numerical results - Biot's modulus

The first parameter of interest is the Biot's modulus.

Theorem 1 (*Biot's Modulus*). *The Biot's modulus in our system,*

$$M = \frac{-1}{Tr(\langle Q_{\mathrm{I}}\rangle_{\mathrm{I}} + \langle Q_{\mathrm{II}}\rangle_{\mathrm{II}})}. \tag{178}$$

is positive. That is

$$M > 0 \tag{179}$$

Proof. In order to prove this we only need to prove that the denominator of M is less than zero. We can begin by writing the denominator in index notation

$$\mathrm{Tr}(\langle Q_{\mathrm{I}}\rangle_{\mathrm{I}} + \langle Q_{\mathrm{II}}\rangle_{\mathrm{II}}) = \left\langle \frac{\partial a_i^{\mathrm{I}}}{\partial y_i} \right\rangle_{\mathrm{I}} + \left\langle \frac{\partial a_i^{\mathrm{II}}}{\partial y_i} \right\rangle_{\mathrm{II}}. \tag{180}$$

We can then multiply Eqs. (133) and (135) from the cell problems by a_i^{I}, a_i^{II} and integrate over Ω_{I}, Ω_{II} respectively. That is,

$$\int_{\Omega_{\mathrm{I}}} a_i^{\mathrm{I}} \frac{\partial}{\partial y_j}(C^{\mathrm{I}}_{ijkl}\xi_{kl}(a^{\mathrm{I}}))\mathrm{d}\mathbf{y} + \int_{\Omega_{\mathrm{II}}} a_i^{\mathrm{II}} \frac{\partial}{\partial y_j}(C^{\mathrm{II}}_{ijkl}\xi_{kl}(a^{\mathrm{II}}))\mathrm{d}\mathbf{y} = 0. \tag{181}$$

Integrating by parts we obtain

$$\int_{\Omega_{\mathrm{I}}} \frac{\partial}{\partial y_j}(C^{\mathrm{I}}_{ijkl}\xi_{kl}(a^{\mathrm{I}})a_i^{\mathrm{I}})\mathrm{d}\mathbf{y} - \int_{\Omega_{\mathrm{I}}} C^{\mathrm{I}}_{ijkl}\xi_{kl}(a^{\mathrm{I}})\frac{\partial a_i^{\mathrm{I}}}{\partial y_j}\mathrm{d}\mathbf{y} + \int_{\Omega_{\mathrm{II}}} \frac{\partial}{\partial y_j}(C^{\mathrm{II}}_{ijkl}\xi_{kl}(a^{\mathrm{II}})a_i^{\mathrm{II}})\mathrm{d}\mathbf{y} - \int_{\Omega_{\mathrm{II}}} C^{\mathrm{II}}_{ijkl}\xi_{kl}(a^{\mathrm{II}})\frac{\partial a_i^{\mathrm{II}}}{\partial y_j}\mathrm{d}\mathbf{y} = 0. \tag{182}$$

Then applying the divergence theorem we obtain

$$\begin{aligned}
&\int_{\Gamma_{\mathrm{I}}} C^{\mathrm{I}}_{ijkl}\xi_{kl}(a^{\mathrm{I}})a^{\mathrm{I}}_i \cdot n^{\mathrm{I}}_j \,\mathrm{dS} \\
&+ \int_{\partial\Omega_{\mathrm{I}}\setminus\Gamma_{\mathrm{I}}} C^{\mathrm{I}}_{ijkl}\xi_{kl}(a^{\mathrm{I}})a^{\mathrm{I}}_i \cdot n_j^{\Omega_{\mathrm{I}}\setminus\Gamma_{\mathrm{I}}} \,\mathrm{dS} \\
&- \int_{\Omega_{\mathrm{I}}} C^{\mathrm{I}}_{ijkl}\xi_{kl}(a^{\mathrm{I}})\xi_{ij}(a^{\mathrm{I}})\mathrm{d}\mathbf{y} \\
&+ \int_{\Gamma_{\mathrm{II}}} C^{\mathrm{II}}_{ijkl}\xi_{kl}(a^{\mathrm{II}})a^{\mathrm{II}}_i \cdot n^{\mathrm{II}}_j \,\mathrm{dS} \\
&+ \int_{\partial\Omega_{\mathrm{II}}\setminus\Gamma_{\mathrm{II}}} C^{\mathrm{II}}_{ijkl}\xi_{kl}(a^{\mathrm{II}})a^{\mathrm{II}}_i \cdot n_j^{\Omega_{\mathrm{II}}\setminus\Gamma_{\mathrm{II}}} \,\mathrm{dS} \\
&- \int_{\Omega_{\mathrm{II}}} C^{\mathrm{II}}_{ijkl}\xi_{kl}(a^{\mathrm{II}})\xi_{ij}(a^{\mathrm{II}})\mathrm{d}\mathbf{y} = 0 \qquad (183)
\end{aligned}$$

where $\mathbf{n}_{\mathrm{I}}$, $\mathbf{n}_{\mathrm{II}}$, $\mathbf{n}_{\Omega_{\mathrm{I}}\setminus\Gamma_{\mathrm{I}}}$ and $\mathbf{n}_{\Omega_{\mathrm{II}}\setminus\Gamma_{\mathrm{II}}}$ are the unit normals corresponding to Γ_{I}, Γ_{II}, $\partial\Omega_{\mathrm{I}}\setminus\Gamma_{\mathrm{I}}$ and $\partial\Omega_{\mathrm{II}}\setminus\Gamma_{\mathrm{II}}$. The terms on the boundaries cancel due to periodicity and then using Eqs. (134) and (136) from the cell problems we obtain

$$\begin{aligned}
&-\int_{\Gamma_{\mathrm{I}}} a^{\mathrm{I}}_i n^{\mathrm{I}}_i \,\mathrm{dS} - \int_{\Omega_{\mathrm{I}}} \xi_{ij}(a^{\mathrm{I}})C^{\mathrm{I}}_{ijkl}\xi_{kl}(a^{\mathrm{I}})\mathrm{d}\mathbf{y} \\
&-\int_{\Gamma_{\mathrm{II}}} a^{\mathrm{II}}_i n^{\mathrm{II}}_i \,\mathrm{dS} - \int_{\Omega_{\mathrm{II}}} \xi_{ij}(a^{\mathrm{II}})C^{\mathrm{II}}_{ijkl}\xi_{kl}(a^{\mathrm{II}})\mathrm{d}\mathbf{y} = 0. \qquad (184)
\end{aligned}$$

Accounting for $\mathbf{y}$-periodicity the first and third integrals above are equal to the corresponding integrals (with corresponding normals) on the boundaries $\partial\Omega_{\mathrm{I}}$ and $\partial\Omega_{\mathrm{II}}$, so that we can apply the divergence theorem in reverse to obtain

$$\begin{aligned}
&-\int_{\Omega_{\mathrm{I}}} \frac{\partial a^{\mathrm{I}}_i}{\partial y_i}\mathrm{d}\mathbf{y} - \int_{\Omega_{\mathrm{II}}} \frac{\partial a^{\mathrm{II}}_i}{\partial y_i}\mathrm{d}\mathbf{y} - \int_{\Omega_{\mathrm{I}}} \xi_{ij}(a^{\mathrm{I}})C^{\mathrm{I}}_{ijkl}\xi_{kl}(a^{\mathrm{I}})\mathrm{d}\mathbf{y} \\
&-\int_{\Omega_{\mathrm{II}}} \xi_{ij}(a^{\mathrm{II}})C^{\mathrm{II}}_{ijkl}\xi_{kl}(a^{\mathrm{II}})\mathrm{d}\mathbf{y} = 0. \qquad (185)
\end{aligned}$$

We can write this as

$$\begin{aligned}
-\int_{\Omega_{\mathrm{I}}} \frac{\partial a^{\mathrm{I}}_i}{\partial y_i}\mathrm{d}\mathbf{y} - \int_{\Omega_{\mathrm{II}}} \frac{\partial a^{\mathrm{II}}_i}{\partial y_i}\mathrm{d}\mathbf{y} &= \int_{\Omega_{\mathrm{I}}} \xi_{ij}(a^{\mathrm{I}})C^{\mathrm{I}}_{ijkl}\xi_{kl}(a^{\mathrm{I}})\mathrm{d}\mathbf{y} \\
&+ \int_{\Omega_{\mathrm{II}}} \xi_{ij}(a^{\mathrm{II}})C^{\mathrm{II}}_{ijkl}\xi_{kl}(a^{\mathrm{II}})\mathrm{d}\mathbf{y}. \qquad (186)
\end{aligned}$$

Since the two terms on the right hand side are positive, we therefore have that

$$-\int_{\Omega_{\mathrm{I}}} \frac{\partial a^{\mathrm{I}}_i}{\partial y_i}\mathrm{d}\mathbf{y} - \int_{\Omega_{\mathrm{II}}} \frac{\partial a^{\mathrm{II}}_i}{\partial y_i}\mathrm{d}\mathbf{y} < 0 \qquad (187)$$

and so using the integral average notation we have

$$\left\langle \frac{\partial a^{\mathrm{I}}_i}{\partial y_i} \right\rangle_{\mathrm{I}} + \left\langle \frac{\partial a^{\mathrm{II}}_i}{\partial y_i} \right\rangle_{\mathrm{II}} < 0. \qquad (188)$$

Since the denominator is less than zero we therefore have that $M > 0$. That is, the Biot's modulus is positive.

We will now carry out the numerical simulations using Comsol Multiphysics to investigate the Biot's Modulus and again the results will show that it is indeed positive. We solve cell problems (133)–(134) and (135)–(136) to determine Q_{I} and Q_{II} in order to compute the coefficient. We first consider the Biot's Modulus with increasing porosity in the case where the matrix has a fixed volume fraction of 45% and we vary the volume fraction of the inclusion to alter the fluid volume fraction. We have that the inclusion has Young's modulus 35 kPa and the matrix has Young's modulus 80 kPa. These values have been chosen at random with the matrix stiffer but on the same order of magnitude to highlight the effect of different properties of the phases. We have plotted the Biot's Modulus for porosities 5%–54% for a variety of Poisson ratios from 0.2–0.49, where we assume that both the matrix and inclusion have the same Poisson ratio.

In Figs. 7 and 8 we see that the Biot's modulus increases with increasing porosity. The quantity $\mathrm{Tr}(\langle Q_{\mathrm{I}}\rangle_{\mathrm{I}} + \langle Q_{\mathrm{II}}\rangle_{\mathrm{II}})$ represents the solid

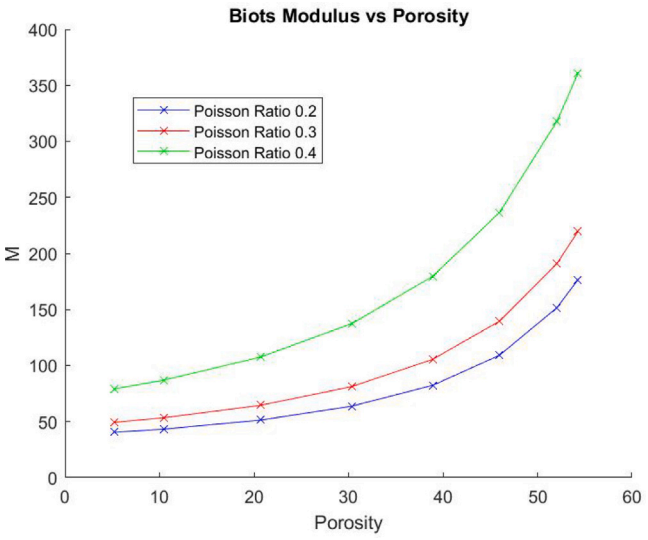

Fig. 7. Biot's modulus vs porosity for Poisson ratio 0.2, 0.3 and 0.4.

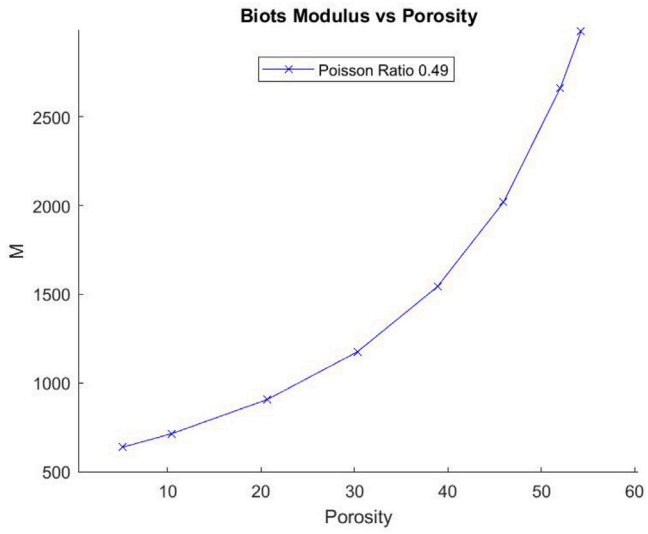

Fig. 8. Biot's modulus vs porosity.

volume variation of the elastic phases, and actually approaches zero. This means that M approaches $+\infty$ as the porosity increases (or equivalently as the solid phases volume fractions approach zero). Here we have the results when both phases have a Poisson ratio of either 0.2, 0.3, 0.4 or 0.49. When both are 0.2 this means that both the phases are fairly compressible and therefore show a larger variation in volume resulting in an overall lower Biot's modulus than when compared with much more incompressible materials. With each increasing Poisson ratio we are making the matrix less compressible. Therefore we see that the Biot's modulus is increasing with increasing porosity and point-by-point is higher for each increasing Poisson ratio. In Fig. 8 the simulations are carried out by assuming that the matrix and fibre network are both almost incompressible. This means that there is very little variation in the solid volume so the denominator of the Biot's modulus expression is extremely small and this therefore results in the very high Biot's modulus shown.

We can also compare how the Biot's modulus relates to the Poisson ratio of the material for a variety of porosities from $\approx 10\%$–$\approx 54\%$. This plot, Fig. 9, again shows the relationship between increasing Poisson ratio of the solid phases and the increase in the Biot's modulus. Each

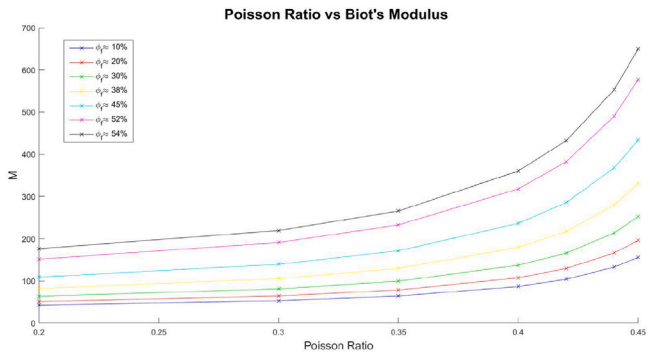

Fig. 9. Poisson ratio vs Biot's modulus.

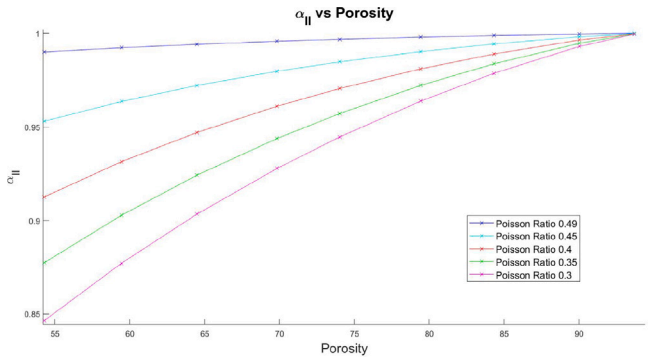

Fig. 10. $\hat{\boldsymbol{\alpha}}_{II}$ vs porosity for different Poisson ratios.

line is a different porosity and the increasing porosity corresponds to a higher value of the Biot's modulus. This reinforces the physical interpretation that the less compressible the solid phases are, the higher the value of the Biot's modulus. The Biot's modulus is higher for the higher porosities as the fluid in the pores is incompressible so the larger the pores the greater the influence they have on the solid phases. For a small porosity then any variation in the solid volume is truly down to the compressibility or incompressibility of the solid phase itself.

5.2.3. Numerical results - Biot's tensor of coefficients

The second poroelastic coefficient that we would like to consider in our analysis is based upon the Biot's tensor of coefficients. We note however that due to the microstructure of our considered material we cannot have a formal Biot's tensor of coefficients with classical upper bound 1 as the elastic phases are fully decoupled. We defined reminiscent Biot's tensors of coefficients for each of the solid phases in (153). Since we do not have the continuity of elastic phases we cannot define one Biot's tensor of coefficients for the entire system. In order to obtain relevant and accurate results we can instead consider individual Biot's tensors of coefficients by considering (161) and 'switching off' the strains firstly in the matrix so that we have the Biot's tensor for only the fibre network $\hat{\boldsymbol{\alpha}}_{I}$ and secondly in the fibres so that we have the Biot's tensor for only the matrix $\hat{\boldsymbol{\alpha}}_{II}$. We can define these tensors as follows

$$\hat{\boldsymbol{\alpha}}_{I} = \phi \mathbf{I} - \langle \mathrm{Tr}(\mathbb{M}_{I}) \rangle_{I} \quad \text{and} \quad \hat{\boldsymbol{\alpha}}_{II} = \phi \mathbf{I} - \langle \mathrm{Tr}(\mathbb{M}_{II}) \rangle_{II} \tag{189}$$

We should note that due to the chosen geometry of our cell the individual Biot's tensors of coefficients (189) is diagonal due to cubic symmetry of the tensors $\mathbb{M}_{I}$ and $\mathbb{M}_{II}$. We can therefore write that

$$\mathrm{Tr}(\mathbb{M}_{I}) = M^{I}_{ijkl}\delta_{lk} = (M^{I}_{1111} + 2M^{I}_{1122})\delta_{ij} \tag{190}$$

and

$$\mathrm{Tr}(\mathbb{M}_{II}) = M^{II}_{ijkl}\delta_{lk} = (M^{II}_{1111} + 2M^{II}_{1122})\delta_{ij}. \tag{191}$$

This means we can write

$$\hat{\boldsymbol{\alpha}}_{I} = \alpha_{I}\mathbf{I} \quad \text{and} \quad \hat{\boldsymbol{\alpha}}_{II} = \alpha_{II}\mathbf{I} \tag{192}$$

where the scalar coefficients can be written as

$$\begin{aligned} \alpha_{I} &= \phi - \langle M^{I}_{1111} + 2M^{I}_{1122} \rangle_{I} \\ \alpha_{II} &= \phi - \langle M^{II}_{1111} + 2M^{II}_{1122} \rangle_{II}. \end{aligned} \tag{193}$$

We consider how the Biot's tensors for each phase, $\hat{\boldsymbol{\alpha}}_{I}$ and $\hat{\boldsymbol{\alpha}}_{II}$, varies with increasing porosity for Poisson ratios 0.3, 0.35, 0.4, 0.45 and 0.49. In the first case we consider just the matrix component which has 3 interconnected cylinders removed and we increase the porosity by increasing the diameter of the removed cylinders from 0.3 to 0.495. In Fig. 10 we can see the results of the Biot's tensor of coefficients $\hat{\boldsymbol{\alpha}}_{II}$ for five different Poisson ratios versus increasing porosity. As the porosity approaches 100% the Biot's tensor for the matrix exhibits the classical behaviour of porous media by tending towards one. The Biot's tensor is the ratio of fluid to solid volume changes at constant volumetric pressure. The coefficient is shown in Fig. 10 to approach one, it can reach identically one for all porosities when the Poisson ratio of the solid matrix is 0.5. Overall the increase in porosity leads to an increase in the incompressible fluid volume in the pores and equally a decrease in the matrix that is still somewhat compressible depending upon the choice of Poisson ratio. This means that the Biot's tensor is linked to both the porosity and the Poisson ratio of the matrix part and both of these influence the rate at which it approaches one.

We are now considering the opposite setup, by considering three interconnected cylinders surrounded by the fluid, where the porosity in this case means the fluid volume in the unit cube surrounding the solid. The solid interconnected cylinders vary in radius from 0.09 to 0.267 to create the variation in the porosity. This is indeed no longer the geometrical setup of porous media so we expect to not obtain the classical behaviour of the Biot's tensor. In Fig. 11 we are considering the opposite to above and so we also see a very different behaviour. Again we are studying the Biot's tensor which is the ratio of fluid to solid volume changes at constant volumetric pressure. However, here we are not considering the typical flow in a porous matrix that gives rise to a classical Biot's tensor that increases towards 1. We instead are considering the flow around 3 orthogonally interconnected cylinders. We can see that for all Poisson ratios except 0.3 that the Biot's tensor decreases towards a lower bound of 1 with increasing porosity. In the case of Poisson ratio 0.3 we see that the coefficient actually increases slightly with the increase in porosity yet still tends towards 1. We can explain this in the following way. When the Poisson ratio is closer to 0.5 then both the solid and the fluid are incompressible and therefore the Biot's tensor would be 1. We however begin our analysis from a solid with Poisson ratio 0.49, so this is not fully incompressible so can have a very small variation in volume. At low porosity the solid volume plays a bigger role in influencing the overall value of the ratio hence the larger value. As the solid decreases in volume fraction (or equivalently the porosity increases) the Poisson ratio approaches 1 as the influence of the very small variation in solid volume plays less of a role and the fluid that is completely incompressible increases in volume. The lower the Poisson ratio the more compressible the solid material is. So when we have Poisson ratio 0.3 the variations can be much bigger meaning that when considering $\hat{\boldsymbol{\alpha}}_{I}$ at 55% porosity we get a Biot's tensor already below 1 and as the volume of the solid decreases (increasing porosity) the ratio again approaches 1 as the influence of the solid variations becomes less important and the fluid incompressibility takes over.

5.3. Scheme for solving macroscale model

We aim to provide a clear step-by-step guide to finding our effective coefficients and solving our global scale model (156)–(161) encoding

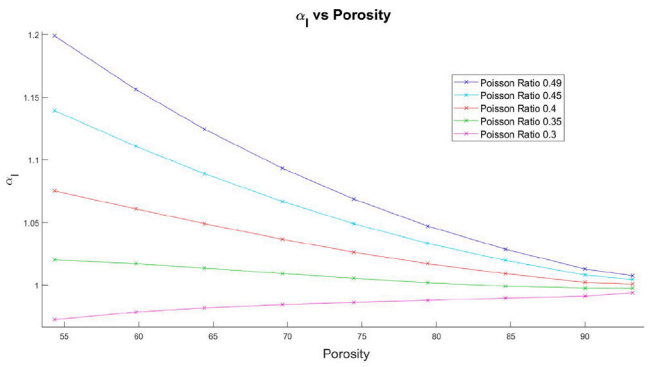

Fig. 11. $\hat{\alpha}_{\mathrm{I}}$ vs porosity for different Poisson ratios.

structural details from across the scales. We also provide, where available, particular references that would assist the reader with the type of numerical simulations that would need to be carried out. Since we have made the assumption of global scale uniformity of the material then we can propose the following steps to solve the model. The process is as follows:

1. We begin by fixing the original material properties of the elastic matrix and the elastic fibres at the microscale. Under the assumption of isotropy we are required to fix parameters for the matrix and the fibres. These parameters are two independent elastic constants e.g the Poisson ratio and Young's modulus (or alternatively the Lamé constants).
2. The microscale geometry then must be defined and we fix the geometry of a single periodic cell at this stage.
3. We would then be able to solve the elastic-type cell problems (129)–(130), (131)–(132), (133)–(134) and (135)–(136) to obtain the auxiliary tensors $\mathbb{M}_{\mathrm{I}}$, $\mathbb{M}_{\mathrm{II}}$, Q_{I} and $\mathbb{Q}_{\mathrm{II}}$ which appear in the macroscale model coefficients. The cell problems to be solved are, in components

$$\frac{\partial}{\partial y_j}\left(C^{\mathrm{I}}_{ijpq}\xi^{kl}_{pq}(A^{\mathrm{I}})\right)+\frac{\partial C^{\mathrm{I}}_{ijkl}}{\partial y_j}=0 \quad \text{in} \quad \Omega_{\mathrm{I}} \tag{194}$$

$$C^{\mathrm{I}}_{ijpq}\xi^{kl}_{pq}(A^{\mathrm{I}})n^{\mathrm{I}}_j+C^{\mathrm{I}}_{ijpq}n^{\mathrm{I}}_j=0 \quad \text{on} \quad \Gamma_{\mathrm{I}} \tag{195}$$

and

$$\frac{\partial}{\partial y_j}\left(C^{\mathrm{II}}_{ijpq}\xi^{kl}_{pq}(A^{\mathrm{II}})\right)+\frac{\partial C^{\mathrm{II}}_{ijkl}}{\partial y_j}=0 \quad \text{in} \quad \Omega_{\mathrm{II}} \tag{196}$$

$$C^{\mathrm{II}}_{ijpq}\xi^{kl}_{pq}(A^{\mathrm{II}})n^{\mathrm{II}}_j+C^{\mathrm{II}}_{ijpq}n^{\mathrm{II}}_j=0 \quad \text{on} \quad \Gamma_{\mathrm{II}} \tag{197}$$

and

$$\frac{\partial}{\partial y_j}\left(C^{\mathrm{I}}_{ijpq}\xi_{pq}(\mathbf{a}^{\mathrm{I}})\right)=0 \qquad \text{in} \quad \Omega_{\mathrm{I}} \tag{198}$$

$$C^{\mathrm{I}}_{ijpq}\xi_{pq}(\mathbf{a}^{\mathrm{I}})n^{\mathrm{I}}_j+n^{\mathrm{I}}_j=0 \qquad \text{on} \quad \Gamma_{\mathrm{I}} \tag{199}$$

and

$$\frac{\partial}{\partial y_j}\left(C^{\mathrm{II}}_{ijpq}\xi_{pq}(\mathbf{a}^{\mathrm{II}})\right)=0 \qquad \text{in} \quad \Omega_{\mathrm{II}} \tag{200}$$

$$C^{\mathrm{II}}_{ijpq}\xi_{pq}(\mathbf{a}^{\mathrm{II}})n^{\mathrm{II}}_j+n^{\mathrm{II}}_j=0 \qquad \text{on} \quad \Gamma_{\mathrm{II}} \tag{201}$$

where we have used the notation

$$\xi^{kl}_{pq}(A^{\mathrm{I}})=\frac{1}{2}\left(\frac{\partial A^{\mathrm{I}}_{pkl}}{\partial y_q}+\frac{\partial A^{\mathrm{I}}_{qkl}}{\partial y_p}\right); \tag{202}$$

$$\xi^{kl}_{pq}(A^{\mathrm{II}})=\frac{1}{2}\left(\frac{\partial A^{\mathrm{II}}_{pkl}}{\partial y_q}+\frac{\partial A^{\mathrm{II}}_{qkl}}{\partial y_p}\right). \tag{203}$$

$$\xi_{pq}(\mathbf{a}^{\mathrm{I}})=\frac{1}{2}\left(\frac{\partial a^{\mathrm{I}}_p}{\partial y_q}+\frac{\partial a^{\mathrm{I}}_q}{\partial y_p}\right); \tag{204}$$

$$\xi_{pq}(\mathbf{a}^{\mathrm{II}})=\frac{1}{2}\left(\frac{\partial a^{\mathrm{II}}_p}{\partial y_q}+\frac{\partial a^{\mathrm{II}}_q}{\partial y_p}\right). \tag{205}$$

The solution of the problems (194)–(195) and (196)–(197) can be obtained by solving six elastic-type cell problems by fixing the couple of indices $k, l = 1, 2, 3$. By doing this we can see $\zeta^{kl}_{pq}(A^{\mathrm{I}})$ and $\zeta^{kl}_{pq}(A^{\mathrm{II}})$ represent a strain and that for each fixed couple of indices k, l we have a linear elastic problem. The problems (198)–(199) and (200)–(201) are vector problems with driving forces being the normals to the interface between either the matrix and the void or the fibre network and the void depending on which problem you are solving. The normal encodes the geometry of the voids and is used to compute the solution.

4. We also require one more condition to ensure uniqueness of solution. We can enforce that the cell averages of the cell problem solutions are zero i.e

$$\langle A_{\mathrm{I}}\rangle_{\mathrm{I}}=0, \quad \langle A_{\mathrm{II}}\rangle_{\mathrm{II}}=0$$
$$\langle \mathbf{a}_{\mathrm{I}}\rangle_{\mathrm{I}}=0, \quad \langle \mathbf{a}_{\mathrm{II}}\rangle_{\mathrm{II}}=0 \tag{206}$$

5. We also must solve the fluid cell problems (103)–(105) to obtain the tensors W, G and L and the vectors $\mathbf{P}$, $\mathbf{H}$ and $\mathbf{S}$ which appear in the macroscale coefficients. The cell problems to be solved are, in components

$$\frac{\partial^2 \mathsf{W}_{ji}}{\partial y_k \partial y_k}-\frac{\partial P_i}{\partial y_j}+\delta_{ij}=0 \quad \text{in} \quad \Omega_{\mathrm{f}} \tag{207}$$

$$\frac{\partial \mathsf{W}_{ij}}{\partial y_i}=0 \quad \text{in} \quad \Omega_{\mathrm{f}} \tag{208}$$

$$\mathsf{W}_{ij}=0 \quad \text{on} \quad \Gamma_{\mathrm{I}} \tag{209}$$

$$\mathsf{W}_{ij}=0 \quad \text{on} \quad \Gamma_{\mathrm{II}}, \tag{210}$$

and

$$\frac{\partial^2 \mathsf{G}_{ji}}{\partial y_k \partial y_k}=\frac{\partial H_i}{\partial y_j} \quad \text{in} \quad \Omega_{\mathrm{f}} \tag{211}$$

$$\frac{\partial \mathsf{G}_{ij}}{\partial y_i}=0 \quad \text{in} \quad \Omega_{\mathrm{f}} \tag{212}$$

$$\mathsf{G}_{ij}=\delta_{ij} \quad \text{on} \quad \Gamma_{\mathrm{I}} \tag{213}$$

$$\mathsf{G}_{ij}=0 \quad \text{on} \quad \Gamma_{\mathrm{II}}, \tag{214}$$

and

$$\frac{\partial^2 \mathsf{L}_{ji}}{\partial y_k \partial y_k}=\frac{\partial S_i}{\partial y_j} \quad \text{in} \quad \Omega_{\mathrm{f}} \tag{215}$$

$$\frac{\partial \mathsf{L}_{ij}}{\partial y_i}=0 \quad \text{in} \quad \Omega_{\mathrm{f}} \tag{216}$$

$$\mathsf{L}_{ij}=0 \quad \text{on} \quad \Gamma_{\mathrm{I}} \tag{217}$$

$$\mathsf{L}_{ij}=\delta_{ij} \quad \text{on} \quad \Gamma_{\mathrm{II}}, \tag{218}$$

6. The auxiliary tensors arising form the cell problems ($\mathbb{M}_{\mathrm{I}}$, $\mathbb{M}_{\mathrm{II}}$, Q_{I} and $\mathbb{Q}_{\mathrm{II}}$, W, G and L) can then be used to determine the global scale model coefficients.
7. The geometry at the macroscale then must be prescribed. The boundary conditions for the homogenized cell boundary must also be given, and the system is to be supplemented with initial conditions for the macroscale solid displacement and pressure.
8. Finally, the macroscale model can then be solved.

6. Conclusion

In this work we have derived a novel system of partial differential equations describing the effective mechanical behaviour of a composite where there is a discontinuity between the elastic phases which are interacting with a fluid phase. Our structure comprises an elastic matrix with a Newtonian fluid that flows in the pores as well as the strengthening elastic fibres that are within the pores and fully surrounded by

the fluid. We remark that the novelty of this work is that the two solid phases are fully decoupled from each other, and therefore we are considering two elastic materials separated by a fluid. This means that we get a poroelastic problem for each solid and fluid when ignoring the other solid constituent and fluid problems that take into consideration how both solids influence that fluid. We can apply this type of structure to many real-world examples, including modelling biological tissues and medical devices.

We began the derivation of the new model by creating the fluid–structure interaction (FSI) problem that appropriately describes the geometry. We close the problem by applying the continuity of stresses and velocities on the interfaces between matrix and the fluid and the fibres and the fluid. We note that there is no continuity of stresses or displacements between the different elastic phases as there is no point of contact. Then by enforcing the length scale separation between the porescale (where all individual phases are clearly visible) and the macroscale (average length of the material) we are able to apply the asymptotic homogenization technique. We apply the technique to the non-dimensionalized FSI problem which allows to obtain the macroscale system of governing equations for our material. We have recovered previously known models in the literature by considering a particular limit case of our model. That is, by enforcing contact between the elastic phases then the model reduces to Miller and Penta (2020). The novel model coefficients encode the precise microstructural details. These coefficients are computed by solving the novel differential problems that arise from using the asymptotic homogenization technique. We finally provide some applications for the model and discuss how the model can be solved numerically.

The novel, pseudo double-poroelasticity model obtained in this work cannot be deduced as a special case of Miller and Penta (2020). This is due to the fact that the discontinuity of the elastic phases changes the nature of the differential cell problems and consequently the model coefficients are different. That is, this model is able to account for the behaviour of two different elastic phases and the influence they have on the fluid that is travelling in the void between them. The model can however be considered as a next natural step in deriving computationally feasible models with complicated microstructures realistic of real-life problems. The key novelty of this work resides in considering the influence of two different discontinuous elastic phases on the fluid that is contained between them. This is reflected in the fluid cell problems (103), (104), (105). Solving these cell problem encodes the details of the geometry and stiffness of the microstructure in the tensors which appear in the fluid flow equation and the conservation of mass equation in the macroscale model. So that is, we are accounting for the microscale complexity within the novel macroscale model. We also have the addition of two new balance equations that are required to close the problem since we do not have the continuity of elastic phases. These new balance equations consider each phase and contain surface integrals of terms arising from the fluid cell problems. This means that we are taking into consideration each elastic phase and the influence of the fluid on it separately. The novel model here cannot be strictly described as *poroelastic-type*, as defined in Miller and Penta (2020).

We noted in the introduction that a similar approach has been taken in Santos et al. (2006) where fractures of porous media are investigated using the asymptotic homogenization technique. The structure in their work involves two different elastic phases and a fluid phase, but is restricted to a simplified geometry where one of the solid phases envelops the other. This means that there is only one solid phase (the internal one) in contact with the fluid. The interface between the solid phase and the fluid has continuity of stresses and velocities. Between the two solid phases there is non welded contact assuming that the stresses across that interface are continuous but displacements and/or velocities are discontinuous. The authors in Santos et al. (2006) make the assumption that the displacement and/or velocity discontinuities are proportional to the stresses across the interface. The proportionality factors are tensors that are specific stiffness and specific viscosity. This differs dramatically from our geometry as we have a complete discontinuity between the elastic phases which leads to both elastic phases having contact with the fluid. The work (Santos et al., 2006) concludes that the jump in the microscale displacements and/or velocities leads to jumps arising in the corresponding macroscopic displacements and/or velocities in the constitutive relations. They also conclude that as only one of their solid phase has contact with the fluid phase then the governing equation for the fluid reduces to the classical ones derived by Biot.

Our current model has some limitations, the macroscale model has been formulated as quasi-static and in a linearized setting. Generalizing our novel model to include linearized inertia would be simple. This addition would lead to the appearance of additional terms in our macroscale model. The additional terms would be leading order linearized inertia which would appear in the effective balance Eqs. (157) and (159). The addition of these inertial terms can be useful to applications of lung modelling where the acoustic properties can be used to aid the diagnosis of pulmonary diseases (Siklosi et al., 2008; Berger et al., 2014). The extension of this work to a nonlinear elasticity setting is very possible from a theoretical point and would build upon the case of Miller and Penta (2021b). There are however complications with the numerical simulations in this case as the two length scales remain coupled leading to an increased computational load. There have however been progresses made recently to address this problem using artificial neural networks (Dehghani and Zilian, 2021).

In the literature, there have been some works investigating the numerical simulations of the asymptotic homogenization cell problems for linear elastic composites and linear poroelasticity (Penta and Gerisch, 2015; Dehghani et al., 2018). The simulations for a linear poroelastic composite with continuity between the two elastic phases have recently been carried out in Miller and Penta (2023b). These simulations have then been used to investigate the effects of microstructural changes induced by myocardial infarction on the stiffness of the heart in Miller and Penta (2023a). The current work could be progressed in many ways however, potentially the most important of these would be to carry out further numerical simulations and model validation using experimental data, such as measurement from biological tissues.

CRediT authorship contribution statement

Laura Miller: Conceptualization, Formal analysis, Investigation, Methodology, Software, Visualization, Writing – original draft, Writing – review & editing. **Raimondo Penta:** Conceptualization, Formal analysis, Funding acquisition, Investigation, Methodology, Project administration, Resources, Software, Supervision, Visualization, Writing – review & editing.

Declaration of competing interest

The authors declare that they have no known competing financial interests or personal relationships that could have appeared to influence the work reported in this paper.

Data availability

No data was used for the research described in the article.

Acknowledgements

RP is partially supported by EPSRC, UK Grants EP/S030875/1 and EP/T017899/1 and conducted the research according to the inspiring scientific principles of the national Italian mathematics association Indam (“Istituto nazionale di Alta Matematica”). All authors approved the final version of the manuscript.

References

Auriault, J.-L., Boutin, C., Geindreau, C., 2010. Homogenization of Coupled Phenomena in Heterogenous Media, vol. 149. John Wiley & Sons.

Bakhvalov, N., Grigory, P., 1989. Homogenisation Averaging Processes in Periodic Media. Springer, Berlin.

Bakhvalov, N.S., Panasenko, G., 2012. Homogenisation: Averaging Processes in Periodic Media: Mathematical Problems in the Mechanics of Composite Materials, vol. 36. Springer Science & Business Media.

Berger, L., Kay, D., Burrowes, K., Grau, V., Tavener, S., Bordas, R., 2014. A poroelastic model of the lung. arXiv preprint arXiv:1411.1491.

Biot, M.A., 1955. Theory of elasticity and consolidation for a porous anisotropic solid. J. Appl. Phys. 26, 182–185.

Biot, M.A., 1956a. General solutions of the equations of elasticity and consolidation for a porous material. J. Appl. Mech. 23, 91–96.

Biot, M.A., 1956b. Theory of propagation of elastic waves in a fluid-saturated porous solid. II. Higher frequency range. J. Acoust. Soc. Am. 28, 179–191.

Biot, M.A., 1962. Mechanics of deformation and acoustic propagation in porous media. J. Appl. Phys. 33, 1482–1498.

Bottaro, A., Ansaldi, T., 2012. On the infusion of a therapeutic agent into a solid tumor modeled as a poroelastic medium. J. Biomech. Eng. 134, 084501.

Bukac, M., Yotov, I., Zakerzadeh, R., Zunino, P., 2015. Effects of poroelasticity on fluid-structure interaction in arteries: A computational sensitivity study. In: Modeling the Heart and the Circulatory System. Springer International Publishing, pp. 197–220.

Burridge, R., Keller, J.B., 1981. Poroelasticity equations derived from microstructure. J. Acoust. Soc. Am. 70, 1140–1146.

Carrillo, F.J., Bourg, I.C., 2019. A Darcy–Brinkman–Biot approach to modeling the hydrology and mechanics of porous media containing macropores and Deformable Microporous Regions. Water Resour. Res. 55, 8096–8121.

Chalasani, R., Poole-Warren, L., Conway, M.R., Ben-Nissan, B., 2007. Porous orbital implants in enucleation: A systematic review. Surv. Ophthalmol. 52, 145–155.

Cioranescu, D., Donato, P., 1999. An Introduction to Homogenization. In: Oxford Lecture Series in Mathematics and its Applications, vol. 17, Oxford University Press, New York.

Collis, J., Brown, D.L., Hubbard, M., O'Dea, R., 2017. Effective equations governing an active poroelastic medium. Proc. R. Soc. Lond. Ser. A Math. Phys. Eng. Sci..

Cookson, A.N., Lee, J., Michler, C., Chabiniok, R., Hyde, E., Nordsletten, D.A., Sinclair, M., Siebes, M., Smith, N.P., 2012. A novel porous mechanical framework for modelling the interaction between coronary perfusion and myocardial mechanics. J. Biomech. 45, 850–855.

Cowin, S.C., 1999. Bone poroelasticity. J. Biomech. 32, 217–238.

Cowin, S.C., Cardoso, L., 2015. Blood and interstitial flow in the hierarchical pore space architecture of bone tissue. J. Biomech. 48, 842–854.

Cowin, S.C., Gailani, G., Benalla, M., 2009. Hierarchical poroelasticity: Movement of interstitial fluid between porosity levels in bones. Proc. R. Soc. Lond. Ser. A Math. Phys. Eng. Sci. 367, 3401–3444.

Dalwadi, M.P., Griffiths, I.M., Bruna, M., 2015. Understanding how porosity gradients can make a better filter using homogenization theory. Proc. R. Soc. Lond. Ser. A Math. Phys. Eng. Sci. 471.

Davit, Y., Bell, C.G., Byrne, H.M., Chapman, L.A., Kimpton, L.S., Lang, G.E., Leonard, K.H., Oliver, J.M., Pearson, N.C., Shipley, R.J., 2013. Homogenization via formal multiscale asymptoticsand volume averaging:how do the two techniques compare? Adv. Water Resour. 62, 178–206.

Dehghani, H., Noll, I., Penta, R., Menzel, A., Merodio, J., 2020. The role of microscale solid matrix compressibility on the mechanical behaviour of poroelastic materials. Eur. J. Mech. A Solids 83.

Dehghani, H., Penta, R., Merodio, J., 2018. The role of porosity and solid matrix compressibility on the mechanical behavior of poroelastic tissues. Mater. Res. Express 6, 035404.

Dehghani, H., Zilian, A., 2021. ANN-aided incremental multiscale-remodelling-based finite strain poroelasticity. Comput. Mech. 1–24.

Flessner, M.F., 2001. The role of extracellular matrix in transperitoneal transport of water and solutes. Perit. Dial. Int. 21, S24–S29.

Holmes, M.H., 2012. Introduction to Perturbation Methods, vol. 20. Springer Science & Business Media.

Hori, M., Nemat-Nasser, S., 1999. On two micromechanics theories for determining micro-macro relations in heterogeneous solid. Mech. Mater. 31, 667–682.

Hu, Z., Metaxas, D., Axel, L., 2003a. In vivo strain and stress estimation of the heart left and right ventricles from MRI images. Med. Image Anal. 7, 435–444.

Hu, Z., Metaxas, D., Axel, L., 2003b. Left ventricle composite material model for stress–strain analysis. Surg. Simul. Soft Tissue Model. 2673.

Jayaraman, G., 1983. Water transport in the arterial wall—A theoretical study. J. Biomech. 16, 833–840.

Karageorgiou, V., Kaplan, D., 2005. Porosity of 3D biomaterial scaffolds and osteogenesis. Biomaterials 26, 5474–5491.

Klanchar, M., Tarbell, J.M., 1987. Modeling water flow through arterial tissue. Bull. Math. Biol. 49, 651–669.

Kolodgie, F.D., Nakazawa, G., Sangiorgi, G., Ladich, E., Burke, A.P., Virmani, R., 2007. Pathology of atherosclerosis and stenting. Neuroimaging Clin. North Am. 17, 285–301.

Kümpel, H.-J., 1991. Poroelasticity: Parameters reviewed. Geophys. J. Int. 105, 783–799.

Lévy, T., 1979. Propagation of waves in a fluid-saturated porous elastic solid. Internat. J. Engrg. Sci. 17, 1005–1014.

May-Newman, K., McCulloch, A.D., 1998. Homogenization modeling for the mechanics of perfused myocardium. Prog. Biophys. Mol. Biol. 69, 463–481.

Mei, C.C., Vernescu, B., 2010. Homogenization Methods for Multiscale Mechanics. World scientific.

Miller, L., Penta, R., 2020. Effective balance equations for poroelastic composites. Contin. Mech. Thermodyn. 32, 1533–1557.

Miller, L., Penta, R., 2021a. Double poroelasticity derived from the microstructure. Acta Mech. 232, 3801–3823.

Miller, L., Penta, R., 2021b. Homogenized balance equations for nonlinear poroelastic composites. Appl. Sci. 11.

Miller, L., Penta, R., 2023a. Investigating the effects of microstructural changes induced by myocardial infarction on the elastic parameters of the heart. Biomech. Model. Mechanobiol. 22, 1019–1033.

Miller, L., Penta, R., 2023b. Micromechanical analysis of the effective stiffness of poroelastic composites. Eur. J. Mech. A Solids 98, 104875.

Moeendarbary, E., Valon, L., Fritzsche, M., Harris, A.R., Moulding, D.A., Thrasher, A.J., Stride, E., Mahadevan, L., Charras, G.T., 2013. The cytoplasm of living cells behaves as a poroelastic material. Nature Mater. 12, 253–261.

Penta, R., Ambrosi, D., Shipley, R.J., 2014. Effective governing equations for poroelastic growing media. Quart. J. Mech. Appl. Math. 67, 69–91.

Penta, R., Gerisch, A., 2015. Investigation of the potential of asymptotic homogenization for elastic composites via a three-dimensional computational study. Comput. Vis. Sci. 17, 185–201.

Penta, R., Gerisch, A., 2017. An introduction to asymptotic homogenization. In: Multiscale Models in Mechano and Tumor Biology. Springer, pp. 1–26.

Penta, R., Merodio, J., 2017. Homogenized modeling for vascularized poroelastic materials. Meccanica 52, 3321–3343.

Penta, R., Miller, L., Grillo, A., Ramírez-Torres, A., Mascheroni, P., Rodríguez-Ramos, R., 2020. Porosity and diffusion in biological tissues. Recent advances and further perspectives. In: Constitutive Modelling of Solid Continua. Springer, pp. 311–356.

Perrin, E., Bou-Saïd, B., Massi, F., 2019. Numerical modeling of bone as a multiscale poroelastic material by the homogenization technique. J. Mech. Behav. Biomed. Mater. 91, 373–382.

Purslow, P.P., 2008. The extracellular matrix of skeletal and cardiac muscle. In: Collagen: Structure and Mechanics. Springer US, pp. 325–357.

Ramírez-Torres, A., Di Stefano, S., Grillo, A., Rodríguez-Ramos, R., Merodio, J., Penta, R., 2018. An asymptotic homogenization approach to the microstructural evolution of heterogeneous media. Int. J. Non-Linear Mech. 106, 245–257.

Rohan, E., Cimrman, R., 2010. Two-scale modeling of tissue perfusion problem using homogenization of dual porous media. Int. J. Multiscale Comput. Eng. 8.

Rohan, E., Naili, S., Cimrman, R., Lemaire, T., 2012. Multiscale modeling of a fluid saturated medium with double porosity: Relevance to the compact bone. J. Mech. Phys. Solids 60, 857–881.

Rohan, E., Naili, S., Lemaire, T., 2015. Double porosity in fluid-saturated elastic media: Deriving effective parameters by hierarchical homogenization of static problem. Contin. Mech. Thermodyn. 28, 1263–1293.

Rohan, E., Turjanicová, J., Lukeš, V., 2021. Multiscale modelling and simulations of tissue perfusion using the Biot–Darcy–Brinkman model. Comput. Struct. 251.

Sánchez, M.T., Pérez, M.Á., García-Aznar, J.M., 2021. The role of fluid flow on bone mechanobiology: Mathematical modeling and simulation. Comput. Geosci. 25, 823–830.

Santos, J.E., Ravazzoli, C.L., Geiser, J., 2006. On the static and dynamic behavior of fluid saturated composite porous solids: A homogenization approach. Int. J. Solids Struct. 43, 1224–1238.

Siklosi, M., Jensen, O.E., Tew, R.H., Logg, A., 2008. Multiscale modeling of the acoustic properties of lung parenchyma. In: ESAIM: Proceedings, vol. 23. EDP Sciences, pp. 78–97.

Tsivgoulis, G., Safouris, A., Katsanos, A.H., Arthur, A.S., Alexandrov, A.V., 2016. Mechanical thrombectomy for emergent large vessel occlusion: A critical appraisal of recent randomized controlled clinical trials. Brain Behav. 6, e00418.

Wang, H.F., 2017. Theory of Linear Poroelasticity with Applications to Geomechanics and Hydrogeology. Princeton University Press.

Weiner, S., Wagner, D.H., 1998. The material bone: Structure-mechanical function relations. Annu. Rev. Mater. Sci. 28, 271–298.

Weinhaus, A.J., Roberts, K.P., 2005. Anatomy of the human heart. In: Handbook of Cardiac Anatomy, Physiology, and Devices. Humana Press, pp. 51–79.

Whitaker, R.H., 2014. The normal heart: Anatomy of the heart. Medicine 42, 406–408.

Xu, L.-Y., Chen, W.-Y., Zhao, K., Cai, F., Zhang, J.-Z., Chen, G.-X., Jeng, D., 2022. Poro-elastic and poro-elasto-plastic modeling of sandy seabed under wave action. Ocean Eng. 260, 112002.

Zakerzadeh, R., Zunino, P., 2014. Fluid-structure interaction in arteries with a poroelastic wall model. In: 2014 21th Iranian Conference on Biomedical Engineering, ICBME. pp. 35–39.